Original research or treatment paper

Advances in identifying archaeological traces of horn and other keratinous hard tissues

Sonia O'Connor[1], Caroline Solazzo[2,3], Matthew Collins[2]

[1]Archaeological Sciences, Division of AGES, University of Bradford, Bradford, UK, [2]BioArCh, Department of Archaeology, University of York, York, UK, [3]Museum Conservation Institute, Smithsonian Institution, Suitland, MD, USA

Despite being widely utilized in the production of cultural objects, keratinous hard tissues, such as horn, baleen, and tortoiseshell, rarely survive in archaeological contexts unless factors combine to inhibit biodeterioration. Even when these materials do survive, working, use, and diagenetic changes combine to make identification difficult. This paper reviews the chemistry and deterioration of keratin and past approaches to the identification of keratinous archaeological remains. It describes the formation of horn, hoof, baleen, and tortoiseshell and demonstrates how identification can be achieved by combining visual observation under low-power magnification with an understanding of the structure and characteristic deterioration of these materials. It also demonstrates how peptide mass fingerprinting of the keratin can be used to identify keratinous tissues, often to species, even when recognizable structural information has not survived.

Keywords: Horn, Hoof, Baleen, Tortoiseshell, Mineral preservation, Keratin, Peptide mass fingerprint, Mass spectrometry

Introduction

Horn, hoof, baleen, and tortoiseshell are all animal hard tissues that have been exploited as raw materials for functional or decorative applications. They are tough, flexible, mouldable, and fusible natural plastics; bio-composites of the protein keratin and a calcium mineral, the latter being a minor component and probably mostly bioapatite.

Horn has always been widely available and was commonly used in the past as a raw material for the production of cultural objects as diverse as composite bows, drinking vessels, powder horns, and inkwells (MacGregor, 1985, 1991; O'Connor & Duncan, 2002; Richards & Gardiner, 2005), sword handles (Stead, 2006; O'Connor, 2013), helmet panels (Doppelfeld, 1964; Bruce-Mitford & Luscombe, 1974), longbow knocks (Jones, 2003), lantern panes (Richards, 2005), reliquaries (Ryan, 1988) hammer heads, knife and fork handles, spoons, and spectacle frames. Compared to horn, the use of hoof has been more limited; its utility restricted by its size and shape. Whole cattle or horse hooves can be lidded to form boxes or cut for buttons, but smaller sheep or goat hooves have little use other than as toggles or pendant ornaments.

Baleen, the fiber-fringed horny sheets from the mouths of filter-feeding whales (Mysticeti), was probably always available to coastal communities in small quantities through the opportunistic scavenging of stranded whales and later as a by-product of the hunting of various species of baleen whales for products such as oil and meat. There is evidence of exploitation of cetacean material from the Mesolithic (Clark, 1947; Whittle, 2000; Mulville, 2002). Whaling on a commercial scale was undertaken by the Basques as early as the twelfth century (Aguilar, 1986), and as whaling developed so did the demand for baleen. From the late thirteenth century, it was used in the construction of crossbow staves, for armour and tourney equipment (Credland, 1981; Moffat *et al*., 2008). Strips of baleen were used for shaping and supporting items of dress, such as the farthingale, stomachers, and stay busks. Baleen is the 'whalebone' of corsetry (Sorge-English, 2011). By the eighteenth century, baleen was a notable import into the UK from the Dutch whalers (Beck, 1882) but was most widely available at the height of the nineteenth-century whaling industry when additionally it was used in the production of brushes, cricket bat handles,

Correspondence to: Sonia O'Connor, Archaeological Sciences, Division of AGES, University of Bradford, Bradford, West Yorkshire BD7 1DP, UK. Email: s.oconnor@bradford.ac.uk

Received December 2013; revised paper accepted March 2014
DOI 10.1179/2047058414Y.0000000134

umbrella stays, furniture inlays (Stevenson, 1907; West & Credland, 1995; Wilkinson, 2003), and almost any application where sheets, strips, or rods of a tough but flexible material was required. Only two archaeological finds of baleen are known to the authors from the whole of the UK, one from Perth (Moffat *et al*., 2008) and one from Westward Ho (O'Connor & O'Connor, in preparation). The picture is similar in the Netherlands where just three finds of baleen have been published (Bartels, 2005; Rijkelijkhuizen, 2009).

Tortoiseshell is acquired from the hard protective shell of large marine turtles and has always been an expensive import in Europe. Used for luxury items, it is occasionally recovered from Roman and later contexts (O'Connor, 1987; Rijkelijkhuizen, 2009) and is characteristically used for inlays, combs, and other items that show off the mottled figuring of the turtle shell to best advantage. It could be argued that it would be more correct to call this material 'turtle shell' but in the biological literature this is used to refer to the entire shell of the turtle, both the external keratinous shield and the underlying boney plates (Zangerl, 1969; Gilbert *et al*., 2001). In historic texts relating to the acquisition and working of the keratinous scutes (scales) themselves (e.g. Smith, 1770; Siddons, 1837), the single word 'tortoiseshell' is employed. This term remains in wide use today in the curatorial and conservation literature and so will be used here.

When compared to other animal hard tissues, such as bone, antler, and ivory, these keratinous materials are greatly underrepresented in archaeological assemblages, even when taking into account issues of availability. The reasons for this are poor preservation and the problems of identification. Most archaeological evidence of horn working has been in the form of caches of the boney horn cores, either whole or sliced (Wenham, 1964; MacGregor, 1985; Armitage, 1990; MacGregor, 1991) but rarely the horn itself. The extensive excavations at York, UK, for instance, have over the years only recovered a few tens of horn fragments but many hundreds of horn cores.

The perspective of this paper is that of two archaeological scientists and a chemist whose collective experience is largely of European species and burial conditions. It draws together current understanding of the chemistry, structure, and decay of keratin, and reviews and evaluates techniques used in the identification of keratinous hard tissues. It presents the criteria for visual identification from structural features and patterns of deterioration and explores the potential of peptide mass fingerprinting for the identification of very poorly preserved material. By presenting these two quite different investigative methods in the same paper, we aim to show their respective strengths and weaknesses, and the benefits of an integrated methodology.

Keratin biochemistry and structure

Keratinous tissues arise from the dermis and epidermis of the skin, but as the secretion of keratin into the cells (cornification) causes them to die, these are not living tissues. Keratins are fibrous proteins, of which there are two major classes; helically organized alpha-keratins, formed by mammals, birds, and reptiles, and beta-keratins, which have a pleated sheet structure and are only produced by birds and reptiles (McKittrick *et al*., 2012).

Hard (trichocyte) alpha-keratin-made tissues, such as hair, claw, horn, hoof, and baleen, and soft (cytoskeletal) alpha-keratin-made tissues, such as the stratum corneum of the skin, are formed of dimers of type I (acidic) and type II (neutral-basic) proteins aligned into intermediate filaments (Plowman, 2007), embedded in a non-filamentous protein matrix (keratin-associated proteins). Keratin proteins have low sulfur content in comparison to some of the matrix proteins, which are rich in the sulfur amino acid cysteine. The sulfur–sulfur cross-linking between cysteines in the keratin's non-helical end and tail domains and the cysteine-rich keratin-associated proteins contribute to the strength and rigidity of the tissues. 'Hard' keratins have, however, a higher sulfur content than 'soft' keratins, which are also present as minor components in horn and hoof (Solazzo *et al*., 2013b). The structural organization and orientation of the intermediate filaments vary from tissue to tissue and influence their mechanical properties. These filaments are randomly oriented in skin cells, but lie at an angle of 20–30° to the direction of growth in horn cells (Marshall *et al*., 1991), while in the tubules of horse hoof they are aligned in the direction of the tubules and perpendicular to the tubules in the intertubular matrix, helping to resist crack propagation (McKittrick *et al*., 2012).

Beta-keratins are the structural proteins of birds' beak, claw, and feather and reptile skin. They do not occur in mammals and instead of forming intermediate filaments they stack together to produce ß-pleated sheet structures. They intermingle with 'soft' alpha-keratins in the shelled epidermis (carapace and plastron) of turtles (Toni *et al*., 2007; Alibardi *et al*., 2009; Dalla Valle *et al*., 2009; Dalla Valle *et al*., 2013) and the ratio of beta- to alpha-keratins determine the degree of hardness of the scutes (Dalla Valle *et al*., 2009). For instance, the carapace of the hard-shelled Florida redbelly turtle *Pseudemys nelsoni*, has a higher ratio of beta-keratins to alpha-keratins compared to that of the soft-shelled turtle *Apalone spinifer* (Dalla Valle *et al*., 2013). The turtle's beta-keratin proteins are at least half to one-

third the molecular weight of their alpha-keratin counterparts. The central region involved in the beta-sheet structure (4.8–8.3% in turtle's beta-keratins) is highly conserved and rich in proline (P) and valine (V) (Dalla Valle *et al*., 2009).

Hard keratinous tissues also generally contain some amount of calcium phosphate salts, from 0.1% to nearly 15% (dry weight), depending on their form and function. Zones of calcification which help maintain the stiffness or the shape or sharpness of a structure through differential wear, have been noted in cat, lion, and rabbit claw (Pautard, 1964; Halstead, 1974), horn (Hashiguchi & Hashimoto, 1995; Hashiguchi *et al*., 2001) baleen (Pautard, 1970; Szewciw *et al*., 2010), rhinoceros horn (Hieronymus *et al*., 2006) hoof, porcupine quill, and bird beak (Pautard, 1964). Baleen is the most highly calcified of these tissues and the level varies from 1% in minke whale to 14.5% in Sei whale of bioapatite in the non-filamentous matrix (Szewciw *et al*., 2010).

Decay and preservation

The decay of keratin, like that of bone (a composite of protein (collagen and osteocalcin) and mineral (bioapatite)), occurs along three pathways: the chemical deterioration of the organic and the inorganic components, and through biodeterioration. Well-preserved bone, however, is readily recovered from burial environments where horn does not survive at all. This is not just because bone has a much higher mineral content (*ca*. 70 wt%) but because of the intimate way in which the organic and inorganic components are distributed and rigidly packed, affording protection to each other (Collins *et al*., 2002). In even the most mineralized of the keratinous tissues the protein is completely exposed to both chemical and microbial attack. The rate of deterioration due to chemical changes is largely determined by the temperature, moisture content, and pH of the burial environment, although this is complicated by the condition of the material prior to burial and potentially by the processing it has undergone in its transformation from raw material to cultural object. Loss of the mineral component will occur in low pH conditions but it is high pH that will have the most deleterious effect on keratin. However, the major cause of keratin deterioration is rapid biodegradation. In the soil, keratins are degraded by enzymes produced by specialized keratinolytic microorganisms, primarily fungi. At least 300 fungi are known to use keratins as a source of nutrients (Błyskal, 2009), but the mechanisms of attack have only been studied in detail with relationship to hair and wool (Wilson *et al*., 2007, 2010; Solazzo *et al*., 2013a). The fungal enzymes denature the constituent proteins and break the disulphide bridges. Different elements of the hair structure are more or less resistant to this attack but surface erosion, radial penetration, and lateral tunneling by fungal hyphae are accompanied by separation of the hair's structural components, loss of the protective cuticle, the destruction of the matrix protein, then the fibrous protein and, finally, the total collapse of the fiber.

As keratinolytic fungi present in the soil become active upon the addition of keratin, preservation is largely dependent on the inhibition of biodeterioration by environments unfavorable to aerobic fungal activity (e.g. lack of oxygen, low temperatures, limiting pH, very low relative humidity), the presence of biocides, or a combination of the two. Examples include the survival of finger nails and hair in the deeply frozen bodies of the Franklin expedition (Beattie & Geiger, 1987) and the Tyrolean Ice Man (Spindler, 1993), the desiccated sand burials (Dzierzykray-Rogalski, 1986) and embalmed mummies of Ancient Egypt and the acid bog burials of Northern Europe (Brothwell & Gill-Robinson, 2002) with their preserving combination of low pH, dark, anoxic, waterlogged conditions and the antiseptic nature of some of the component vegetation. It is no surprise that woollen textiles and objects in horn and other keratinous tissues are also preserved with many of these inhumations. However, through a combination of sub-aerial weathering and biodeterioration, material left on the ground surface for any length of time will not survive to be incorporated into archaeological deposits in a recognizable form. This is probably why so little keratinous material survives, for instance, in the deep, anoxic, waterlogged deposits of urban sites in York, UK (O'Connor, 1987) or similar sites across Amsterdam, Netherlands (Rijkelijkhuizen, 2009) despite otherwise favorable conditions for preservation. That this absence of evidence is not just evidence of absence but largely an issue of preservation is corroborated by the many examples of traces of horn discovered as mineral preserved organic (MPO) remains during the conservation of metal objects from such sites.

Mineral preserved organic remains

Even in apparently unfavorable burial conditions, keratinous tissues do survive as MPO remains where they have lain in close contact with corroding metals. The metal corrosion products pervade the organic material, coloring, or coating, and/or invading its structures and affording some level of protection to the organic matrix. The survival of plant- and animal-derived MPO remains have long been recognized (Biek, 1963) and this knowledge has both influenced the direction of development of conservation techniques and greatly increased our understanding of the organic components of archaeological

assemblages. Even in anoxic, waterlogged sites such as Coppergate, York, many more instances of MPO horn are found than waterlogged examples, providing a much clearer picture of its widespread use.

The mechanisms of mineral preservation have been explored mostly in relation to wood and textiles in contact with iron and copper alloy in the context of inhumations where these materials are often intimately combined. The extent (or absence) of MPO remains, the form the mineralization takes (positive or negative cast, or both) and the quality of detail preserved depends on factors such as the relative rates of deterioration of the organic and metal components, which organic and metallic materials are involved, the concentration of metal ions in solution, the rate of ion take-up by the organic material, and the constituents of the ground water (Keepax, 1975; Janaway, 1983, 1989; Turgoose, 1989; Gillard *et al.*, 1994). Positive casts, where the metal ions penetrated the cells and fibers of the organic material, produce the best preservation of detail. The corrosion products of several metals have biocidal properties that also help preserve the organic matrix of the material while mineralization proceeds. Foremost among these is copper, although MPO remains on silver and lead have been observed (Edwards, 1974; Stock, 1976). The metal ions released by the oxidation of iron, however, are not toxic to the microbiota and the cascade of iron oxidation products does not passivate the surface, unlike copper. Taken together this means that biodeterioration is not directly affected by iron corrosion, and indeed in some cases can be accelerated by it, but rapidly corroding iron can engulf organic material demonstrably conferring indirect protection.

Fig. 1 is a most spectacular example of the MPO preservation of keratinous material. This is one of two coins that had been placed over the eyelids of an eighteenth-century corpse buried near St John's harbor Newfoundland, Canada, that were recovered with a patch of woollen shroud and eyelashes on either side (Hett, 1980). A slow rate of corrosion has kept the copper ion concentration low and produced positive casts, with minimal green staining, while inhibiting fungal attack of the keratin. The results are MPO remains that have retained much of the appearance, properties, and micro structure of the original materials, including the pigment granules in the eyelashes. This contrasts sharply with the preservation of MPO keratin by corroding iron. Without the protection of a biocide, decay can be so fast that before mineralization has penetrated any distance, the keratinous material is reduced to a formless mush. Recognizable MPO remains may be found, if at all, only as an impression in the corrosion at the original surface of the metal object. For instance, evidence of joins and grain direction of the horn handle components of one of the South Cave Iron Age swords were clearly preserved against the iron tang but the shape and thickness of the guard, grip, and pommel were entirely lost (O'Connor, 2013).

Figure 1 MPO remains of keratinous materials first published in Hett (1980). © Government of Canada, Canadian Conservation Institute, CCI 2003063-0001.

Visual identification

Even when these keratinous materials do survive in the archaeological record they may not be recognized. Horn, for instance, is a material with which we are unfamiliar today, its place having almost entirely been supplanted by synthetic plastics. The shape of a complete horn is perhaps unmistakable but once fragmented, worked, or decayed its identification can be problematic.

Most guides to the identification of worked animal-derived hard tissues are centered on osseous materials with a preoccupation with ivory and its substitutes (Penniman, 1952; Krzyszkowska, 1990). Campbell Pedersen's (2004) book includes a range of keratinous materials and is a very useful resource for the identification of historic objects but is of limited use when faced with degraded archaeological finds. Only a few publications address the identification of archaeological keratin. O'Connor (1987) is mostly based on waterlogged finds recovered from sites in York and Rijkelijkhuizen (2008) on finds from Amsterdam. Florian (1987) briefly describes the features of these materials in the context of their decay in marine environments and Lauffenburger (1993) covers the identification, historic uses, and past conservation treatments of baleen. The work presented here builds on these papers and the results of O'Connor's recent study into the identification of animal hard tissues.

While the identification of MPO remains through scanning electron microscopy is well established (Keepax, 1975; Janaway & Scott, 1983; Watson,

1988), it is not usually necessary for the visual identification of keratinous tissues, however preserved. SEM offers high magnification, excellent depth of field and resolution, and environmental chambers now allow objects to be examined without the need for sampling and coating, but cannot reveal variations in color or translucency. Many of the diagnostic features identified in this paper were visible, in good light, to the unaided eye and have been captured using nothing more sophisticated than a Panasonic Lumix DMC TZ6, a compact digital camera with a good macro facility. The more detailed characterization and recording of these features were undertaken using a Wild Heerbrugg M8 stereomicroscope or a Dino-Lite (AM-7013MZT) 5 megapixel digital microscope with polarizer, at magnifications typically between 20× and 50×, and occasionally at 200×. At higher magnification, these keratinous materials can look very similar, all being formed in part from compressed layers of keratinized epithelial cells. At lower magnifications it is easier to see how these cells are organized in relationship to other more specialized structures and their orientation to any surviving natural surfaces.

Horn

True horns are found only on the skulls of ruminant artiodactyls such as cattle, sheep, goat, and antelope. The bone horn cores grow out from the frontal bone of the skull and the horn develops from its epithelial covering, forming a sheath with a finely layered cone-within-cone structure. Horn has a longitudinal, fibrous grain and the surface may have thin, uneven, circumferential ridges marking the edges of sequential cones, particularly toward the junction with the skull (Fig. 2). The cross section of the horn is determined by that of the horn core and in general is circular to oval in cattle, elliptical in goat, and triangular in sheep although there is much variation in the color, texture, torsion, and external sculpting between different domestic breeds today. Sheep and goat horn can be translucent and virtually colorless while cow horn may have a pale brown or greenish tinge, or be layered and longitudinally streaked with colors ranging from white to reddish brown or black, while buffalo horn is black and opaque.

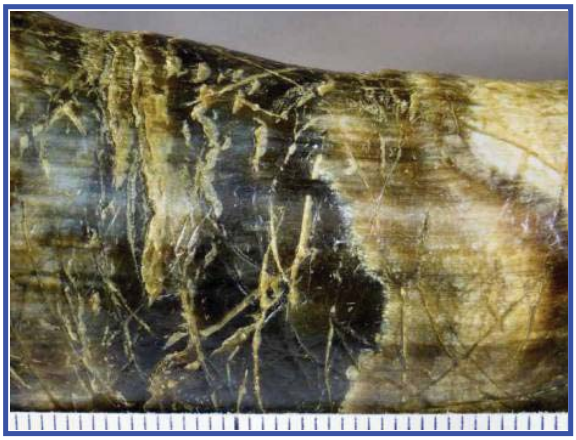

Figure 2 Detail of the naturally worn surface of a cattle horn. © Sonia O'Connor.

The horn accumulates throughout the life of the animal (except that of the pronghorn antelope (*Antilocapra americana*), which sheds its horn sheath annually but retains the horn core) increasing the thickness of the horn over the sheath and developing a solid mass beyond the distal tip of the horn core. The flattened cornified epithelial cells form growth layers over the surface of the horn core. These layers are periodically punctuated by tubules that run the length of the horn and appear as oval or elliptical porosities between the layers in a transverse section. The morphology of the layers and the distribution and size of the pores vary between cattle, sheep, and goat horn and can aid identification even when the shape and color of the horn are altered by working and decay.

Cow and ox horn have very few, relatively inconspicuous pores but the growth layers are wavy with a compact boundary that give the unworked surface a longitudinally corrugated appearance. In worn or worked surfaces these corrugations may still be apparent from the distribution of the pigmentation in the truncated layers (Fig. 2), but pressed and polished translucent horn can look like a homogeneous sheet of plastic. With time, starting at the edges of the horn, deterioration allows air to infiltrate between the layers, making the corrugations visible once again in either reflected or transmitted light. In transverse section, the layers describe a series of intersecting arcs of similar size. These can be particularly obvious toward the centee of the solid part of the horn tip where each layer follows the path of the layer below around a central point and the synchronous intersections of the arcs produce a pattern of radially organized lines between the columns of arcs (Fig. 3A). Moving out from the center, the arcs of each successive layer are minutely longer as the circumference of the horn increases. Eventually a critical length of arc is reached and the next layer has additional arcs. Occasionally two columns of arcs also merge but the overall size and shape of the arcs is maintained throughout the radius of the horn. Buffalo horn has flattened, almost triangular, cross sections and the layers of the horn in the solid tip form around a line of small anomalies, instead of a single point. The layers are finer and the wave produced by the arcs is less distinct and sometimes absent.

Sheep and goat horn is often unpigmented and transparent. The solid tip in transverse section has an elongated or discontinuous central anomaly and

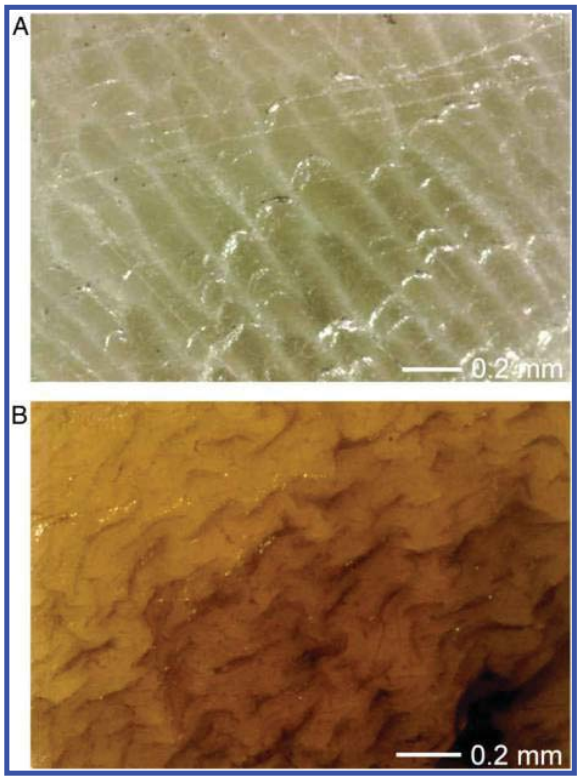

Figure 3 Worked surfaces approximating to the transverse section of the horn tip (A) of cattle (Hawley Collection specimen) and (B) of sheep horn. © Sonia O'Connor.

in some sheep horn the triangular path of the layering around this can distinguish it from goat. The layering does not have the pattern of intersecting arcs and radial lines seen in cattle horn (Fig. 3B). Sheep horn in particular contains many larger pores, that flatten as the horn dries, and the layers follow an undulating path over them. Hanausek (1907, p. 433) records pores of 30–160 μm in sheep horn, while McKittrick *et al.* (2010) record pores of 40 by 100 μm and a mid-range tubule density of 22 mm^{-2}. The horn of the bighorn sheep (*Ovis canadensis*) has evolved to withstand extreme loading impacts during fighting and has been studied in detail (Tombolato *et al.*, 2010). The horn is particularly densely packed with large tubules, up to 200 μm at their maximum diameter, interleaved with layers of horn only 2–5 μm thick.

In dry conditions horn shrinks and concentric and longitudinal cracks open revealing the lamella structure. The compact boundaries of the corrugated layers of cattle horn can be very distinctive at this stage. Deterioration in the soil leads to a loss of color and transparency as the cells of the layers begin to separate and disintegrate. If deterioration continues eventually these sheets degrade to a fibrous longitudinal mass and are lost. In alkaline conditions horn will follow a different diagenetic pathway. Chemical hydrolysis rapidly destroys higher order structure producing a structureless gel that eventually

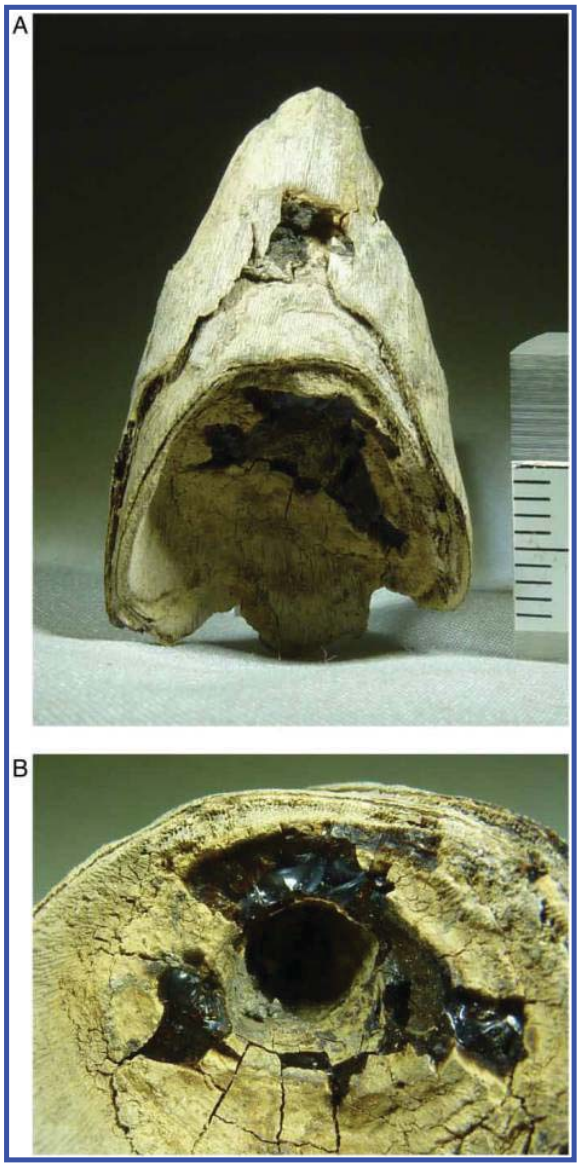

Figure 4 Fragment of horn tip (YAT 1977.7.16022) from waterlogged deposits, (A) side view and (B) interior view (York Archaeological Trust specimen).

dissolves. Even if the further deterioration of this gel was arrested, it is unlikely to be recovered during excavation. In the case of the cattle horn tip fragment in Fig. 4, the corrugated sheet structure is still recognizable but some layers have decayed to a gel that has dried, presumably after excavation, to a hard, resinous material. It is not understood why this has occurred only in certain layers nor are the precise details of the original burial conditions knowable.

Where mineral preservation occurs, this fibrous mass may survive as the metal object and its corrosion provide some physical protection. Stained brown with iron corrosion, MPO horn is often mistaken for wood but examination under low magnification will indicate a complete absence of the cellular organization of wood, particularly ray cells (Fig. 5). With very

Figure 5 Detail of MPO horn remains on an iron knife handle with copper alloy rivets (York Archaeological Trust specimen).

decayed horn a positive identification will require the application of other, more destructive analytical techniques (see below).

Figure 6 Hoof sheath from a horse. © Sonia O'Connor.

Hoof

Hoof forms as a capsule over the distal phalanx of the feet of ungulates and is very similar to horn in color and structure. In horse this is a single structure (Fig. 6) but in cloven-footed animals, such as cattle, the foot ends in two digits and each is covered by a separate sheath or claw. The fine detail of the hoof structure varies depending on the location within the hoof, e.g. the wall or the sole.

Like finger nail, the hoof wall is formed from its proximal edge, the junction between the hoof and the skin of the foot. Here cells are produced by the coronary corium, become cornified and die, and are moved forward over the dermis as new cells are formed behind them. Variations in growth rate can produce slight textural features that ring the hoof horizontally (Fig. 6). The surface of the corium has long papillae from the ends of which tubules form within the intertubular keratin matrix (Fig. 7). The tubules lie parallel to the surface of the hoof and extend from the corium to the base of the wall. This gives the external surface of the hoof wall a finely striated appearance (Fig. 8), the paired strae being the walls of the hollow tubules. Variations in color and translucency of the intertubular matrix may form stripes or streaks in this direction. Toward the proximal edge of dry hoof specimens, successive edges of thin layers of the hoof may be visible and in polished surfaces variation in the color relates both to the tubule direction and changes through the depth of the wall. The sole of the hoof has its own corium that produces a softer more pliable horn material.

Although primarily a tubular structure, the outer portion of the wall has some layering. The fully keratinized intertubular matrix consists of plate-like flattened cells, the longitudinal axes of which lie parallel to the direction of tubule growth (Marshall *et al.*, 1991). The inner surface of the wall is sculptured

Figure 7 Detail of the proximal edge of the horse hoof wall showing the upper ends of the tubules and the white ridges on the interior surface of the wall. © Sonia O'Connor.

Figure 8 Details of the exterior of the horse hoof wall showing the vertical striations formed by the tubules. © Sonia O'Connor.

with unpigmented, vertical ridges (Fig. 9) that interdigitate with the fine leaf-like laminae of the dermis (some 550–600 in horse hoof wall; Pollitt, 2004). Removed from the bone and cleaned of the dermis, this inner surface appears white against the pigmented intertubular matrix of the bulk of the wall and is visible on the exterior of the hoof as a white line between its wall and sole. The lower edge of the hoof wall is worn away by contact with hard surfaces but if the rate of growth outstrips the rate of wear this can cause lameness and other health problems. To avoid this, it is often necessary to trim the hooves of domestic livestock (Fig. 10).

In young, healthy horses the outer surface of the wall is covered in a distinctly smooth and shiny layer (the periople) which flakes away in adult hooves. The papillae of the coronary corium are 4–5 mm long and taper to a point. The holes they leave behind are easily visible to the eye in the concave, upper edge of the wall of the detached hoof (Fig. 7). The tubules these form in the bulk of the hoof wall are oval in cross section and have a well-defined cortex of flattened, unpigmented, keratinized cells arranged concentrically around the medulla (Figs. 8 and 9). Where the cells of the intertubular matrix are darkly pigmented with melanin, the tubules appear particularly prominent (Pollitt, 2004). The tubules increase in diameter but reduce in number from the outer toward the inner region of the wall (Bragulla & Hirschberg, 2003), up to 220×140 μm with a medulla of 50 μm (McKittrick *et al.*, 2012). The

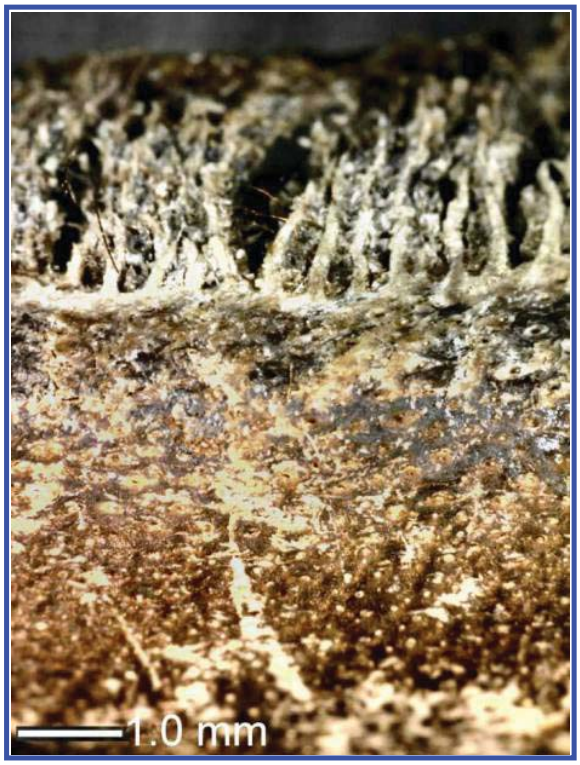

Figure 9 Photomicrograph of the worn lower edge of the horse hoof wall with the white ridges of the interior surface uppermost. © Sonia O'Connor.

Figure 10 Dried clippings from a horse hoof. © Sonia O'Connor.

tubules toward the exterior of the hoof become quite flattened parallel to the surface in a dried specimen. In the region of the largest tubules there is proportionately very little intertubular matrix between them. McKittrick *et al*. (2010) records a mid-range tubule density of 24 tubules per mm^{-2} while Pollitt (2004) reports a decline from 22 to 11 mm^{-2} step-wise toward the inner surface, with an overall mean density of 16 mm^{-2}.

In modern cattle, the hoof wall thickness is *c.* 4–4.5 mm and is formed from between 50 and 60 tubules per mm^{-2}, embedded in the intertubular matrix. In sections of fresh hoof, the tubules nearest the claw surface are flattened parallel to that surface. Deeper in, the tubules are more oval (of the order of 50 μm maximum diameter) but the layer nearest the underlying laminar dermis, is virtually free of tubules, in contrast to horse hoof (Franck *et al.*, 2006). The walls of the tubules are thinner than in horse hoof (McKittrick *et al.*, 2012)

Once removed from the living hoof the keratin capsule loses moisture and shrinks. Hoof clippings trimmed from the base of the wall crack and curl laterally into tight coils with the exterior of the hoof wall to the outside (Fig. 10). For this paper, it was not possible to examine sufficient archaeological examples of known hoof to detail the deterioration but the tubular structure is persistent and can be made more obvious by these changes. Cracks can propagate through the thickness of the hoof between tubules and also between the flattened cells of the intertubular matrix producing delamination roughly parallel to the outer surface. Sections of hoof wall can easily be mistaken for horn but should be distinguishable on the detail of edges perpendicular to the tubules (Figs. 3 and 9). Gelatinization in patches producing irregular holes through the wall of an unworked cattle claw has also been observed from the material at York.

Baleen

Baleen plates are thin, roughly triangular sheets (Fig. 11) of keratinous tissue that hang in racks, like the closely stacked vanes of vertical window blinds, down from the upper jaw on either side of the mouths of the baleen whales. The main plates, the sheets at the outer (labial) edge of the mouth, are the longest and are usually flanked on their inner lingual edge by smaller accessory plates. The fibers, or bristles, of the inner edge of each sheet mesh together with those of adjacent sheets to form a sieve against which the food of the whale is trapped. Sections through a baleen plate reveal a tripartite structure consisting of a covering layer of finely lamellar, horn-like material surrounding a filling of tightly packed, longitudinal tubules, with well-defined

Figure 11 A sheet of baleen (KINCM W7-7-76) lit to show the natural surface texturing (Hull Museums specimen).

cortex and medulla, cemented together by intertubular horn (Halstead, 1974). The horny covering wraps smoothly over the longitudinal edges except where the tongue has worn it away and the tubules are exposed as the bristly fringe. This inner (lingual) edge tapers to the lower (distal) end of the plate, which terminates with a tuft of bristles.

Baleen is formed through the cornification of epithelial cells of the gum and grows continuously. Each main plate corresponds to a transverse dermal ridge in the gum that has numerous extremely long dermal papillae along its edge from which the tubules develop. The keratinized cells of the tubules are flattened parallel to the tubule's surface and oriented concentrically around the medulla. The outer horny covering of the baleen plate consists of flattened, cornified cells arranged in fine layers parallel to the surface of the plates and is formed by the epithelium on the sides of the dermal ridges. The surfaces of the

plates are often striated longitudinally but also show shallow undulations across the width of the plate that may relate to variations in growth rate (Fig. 11). The development and structure of baleen in the fetal and adult whale is covered in detail by Fudge *et al.* (2009), who present an annotated translation of the seminal 1883 paper by Tycho Tullber.

The tubules of a single plate have a range of diameters but the average tubule diameter depends on the species (Figs. 12 and 13). The tubule stiffness also varies between species and is related to the level of calcification (Szewciw *et al.*, 2010). Melanin pigmentation is associated both with the tubules and the covering layers. The size, shape, and thickness of the baleen plates vary with species and their color can be bluish black, brown, or pale honey colored, with longitudinal, darker streaks (Watson, 1981). The color, shape, and size of the plates and the relative bristle density and diameters of different whale species are detailed by Young (2012).

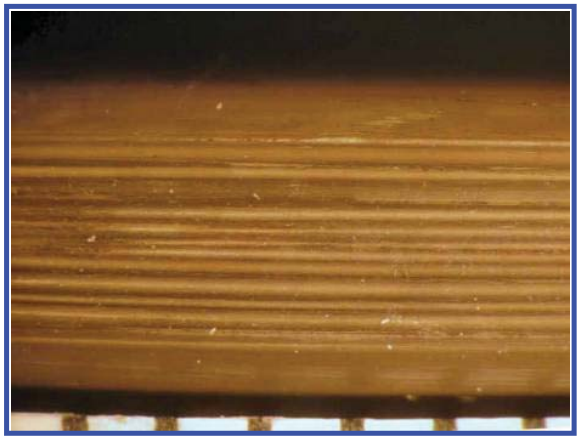

Figure 12 The edge of a baleen stomacher (KINCM 2005-2401) providing a longitudinal section through the thickness of the baleen plate. The tubular layer lies horizontally between the layers of the horny covering (Hull Museums specimen).

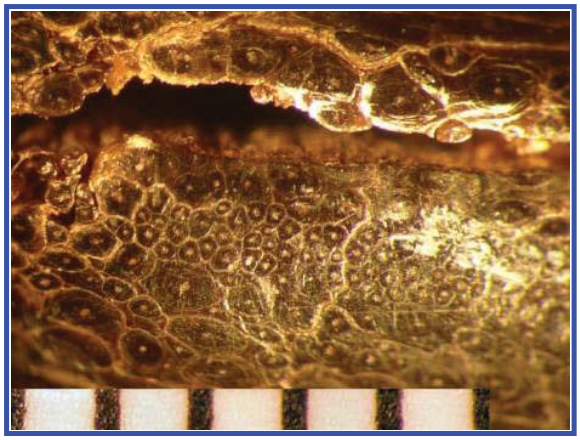

Figure 13 The end of a baleen stomacher (KINCM W5-90-76) providing a transverse section of the tubular layer (Hull Museums specimen).

In worked objects where the tripartite structure is retained, the material is easily identified as this is a feature unique to baleen. Stripped away from the fibrous core, the outer horny covering layers of the baleen can be difficult to distinguish from horn. The size of the sheet may rule out horn and the combination of fine vertical striations and horizontal undulations on the exterior may help confirm identification, if these have not been lost through working (Fig. 11). The layers of horny baleen are finer, flatter, and less fibrous in appearance than cattle or sheep horn. On edges that approximate to a transverse section the layers, although wavy, are not organized into columns of nested corrugations like cattle horn nor are they interspersed with flattened tubules as in sheep horn. On their own, the tubules can be mistaken for a range of mammal hair, depending on their diameter, but under high magnification the surface is seen to be formed from a mosaic of epithelial cells, which vary between species (Pfeiffer, 1992), rather than cuticular scales.

Long exposure to light produces a graying of dark baleen. As baleen dries it shrinks and becomes increasingly stiff and brittle and the tubules become rigid and easily fracture. Thin layers of the horny covering exfoliate along incised designs and cut edges (Fig. 14). On the surface of the plates, oval-shaped blisters can form where the outer layers detach around fine longitudinal splits. In archaeological examples the horny covering layer and tubules usually prove more persistent than the intertubular matrix. The many examples preserved in Arctic permafrost may appear to be in a reasonable condition until they thaw when they are found to have delaminated and become detached from the tubular layer (Wardlaw & Grant, 1994). This was also the case with the two examples found in waterlogged deposits in the UK; a worked object from Westward Ho!

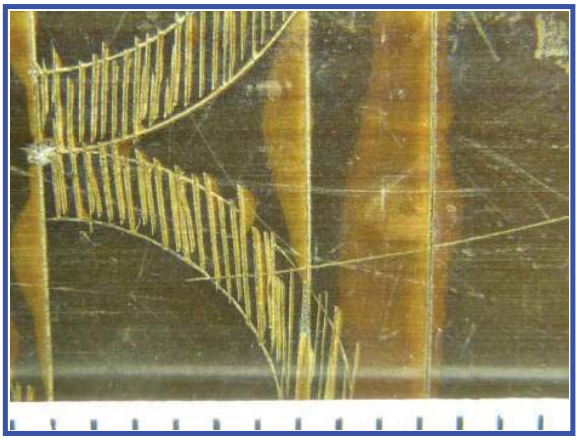

Figure 14 Surface delamination around the incised decoration of a baleen stomacher (46.1983.246 Leeds Museums and Galleries specimen).

Figure 15 Fragment of waterlogged baleen from the Horse Cross site, Perth, Scotland, excavated by the Scottish Urban Archaeological Trust (SUAT) in 2004. © Sonia O'Connor.

(O'Connor, in preparation) and unworked plate fragments (Fig. 15) from Perth (Moffat *et al.*, 2008).

Tortoiseshell

The bodies of tortoises, turtles, and terrapins are encased in protective shells formed from a shield of keratinous scutes (scales) over a boney mosaics of geometric plates. Large marine turtles, most particularly hawksbill turtle (*Eretmochelys imbricate*) but also green turtle (*Chelonia mydas*), produce thick keratinous shields with excellent working properties. These turtles have large thick scutes over the top (vertebral scutes) and sides (pleural scutes) of the carapace (dorsal plate). Although the scutes of this shield can be dark, matt, and algal covered in life, when separated from the bone and worked, the material transforms into glossy, vibrant, translucent, mottled tortoiseshell (Fig. 16). The tortoiseshell of the plain colored scutes of the plastron (ventral plate) is comparatively thin but the scutes are large and this is also utilized for inlays and coverings.

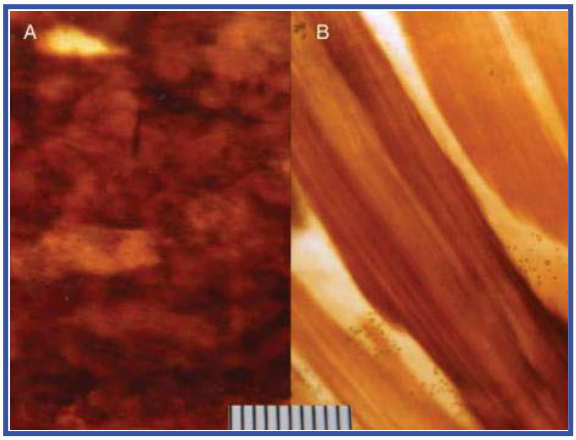

Figure 16 Tortoiseshell from (A) hawksbill turtle and (B) green turtle. © Sonia O'Connor.

The boney mosaic is covered by a germinal layer that forms the scutes but the edges of the scales do not align with the junctions of the boney plates. The polygonal cornified cells of tortoiseshell are flattened parallel to the surface of the germinal layer and coalesce into a compact layer about 20 cells deep. Each layer is separated from the next by a distinct boundary layer that appears to form in response to seasonal changes in metabolic activity. Despite this, the keratinized cells form a quite transparent, pale colored ground. Melanin granules within the cells produce the dark mottling of the tortoiseshell, which is seen throughout the thickness of the material. In many species of turtle the outer (older) layers are periodically shed but in the hawksbill and green turtle the scutes get appreciably thicker over time. As the turtle maintains the same number of scutes throughout its life, the area of successive layers increases as the turtle grows, the discontinuity between successive layers producing the appearance of contour lines on the map of a hill. However, the growth in area of the scute may not be the same in all directions so the thickest part of the scute may be toward one particular edge in some species, rather than centrally located (Hanausek, 1907; Zangerl, 1969; Solomon *et al.*, 1986). The distinctive white pattern of curved, diffuse-edged lines on the underside of the scutes (Fig. 17) is not described in the biological literature but may indicate bands of transitional cells (Dalla Valle *et al.*, 2009) in the process of changing from epithelium to fully cornified shield.

The tortoiseshell of the plastron of hawksbill turtle is plain yellow, although occasionally blotched with black, while that of the green turtle is thinner and varies from yellowish white to dark gray or bluish green in different individuals. The scutes of the carapace are more distinctive and their colors and patterning are central to the identification of each species.

Figure 17 Detail of the natural patterning on the underside of a tortoiseshell scute from a hawksbill turtle. © Sonia O'Connor.

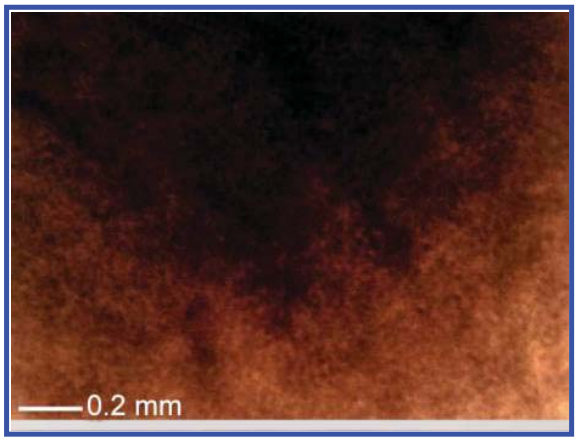

Figure 18 Photomicrograph of the pigment distribution in tortoiseshell from a hawksbill turtle (Horniman Museum specimen).

Those of the hawksbill vary in color between scutes and between different oceanic populations (Hanausek, 1907, pp. 433–435). The translucent background color of this tortoiseshell can be a blonde or pale fawn, sometimes with a hint of green, or golden yellow through to reddish amber, and densely but unevenly mottled with blotches of dark brown or almost black spots (Fig. 16A). These spots can seem randomly spaced or merge to form irregular stripes covering the majority of the surface of the scute. Green turtle carapace scutes can be plain but usually they are patterned with radiating brown stripes as if painted with broad brush strokes (Fig. 16B) from the highest point at the edge of the vertebral and pleural scutes. The background color can vary from pale yellow to dark brown, often with a greenish tinge. Although these patterns of mottling are seemingly very different, it is surprisingly difficult to distinguish the species in a finished object. Not only is this because the size and form of the object may provide only a very limited view of the pattern of mottling but as tortoiseshell can be readily and invisibly fused to itself, the object may be cut from laminated sheets or reformed, randomly oriented scraps. Hanausek, writing in the early twentieth century, notes that the plain colored tortoiseshell of the green turtle is artificially colored to imitate that of hawksbill, which is deemed to be 'true' tortoiseshell (Hanausek, 1907, p. 434).

The light colored ground of tortoiseshell is relatively transparent and featureless. Where this pale ground meets the darker mottling there are no hard boundaries. At its densest the mottling may be quite

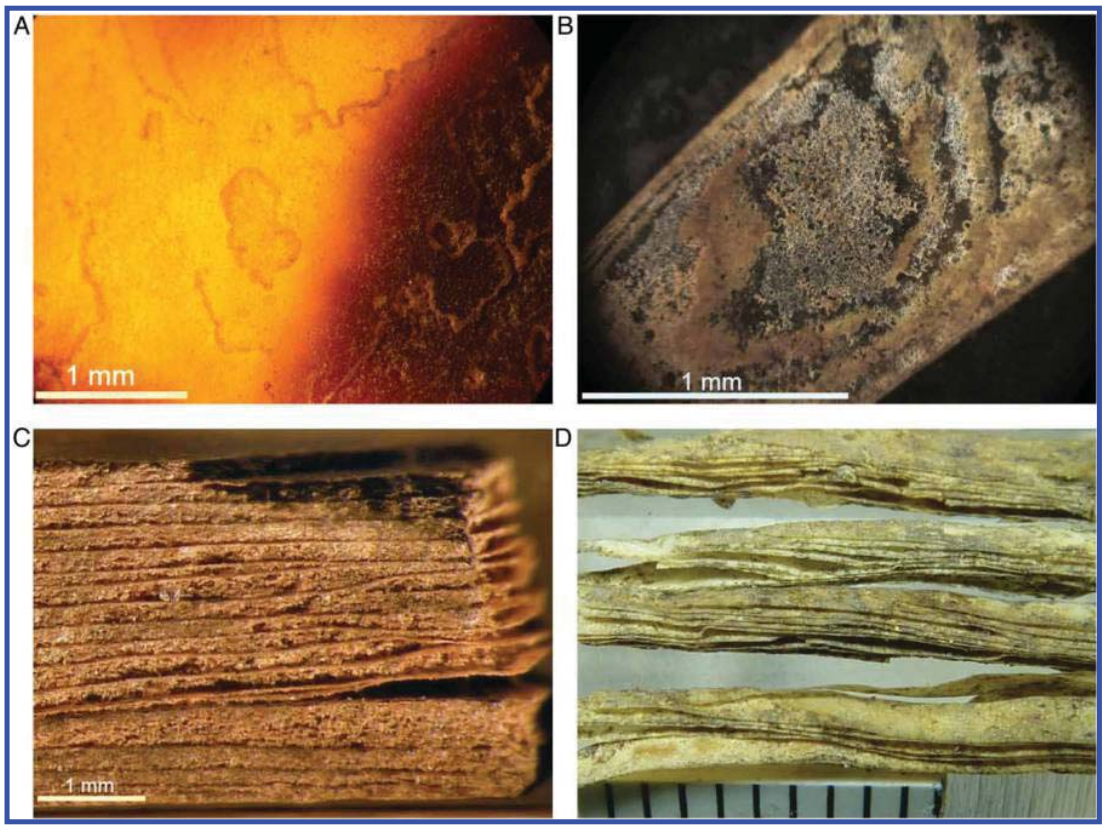

Figure 19 Successive stages in the deterioration of worked tortoiseshell, (A) loss of cohesion at the edges of the layers (Hawley collection specimen), (B) surface delamination and degradation (WCM 100879 sf 60), (C) degraded layers throughout the thickness of the material, viewed from the edge (Hawley collection specimen), (D) loss of degraded cells leaving only the boundary layers (2006.5201.923 kind permission of York Archaeological Trust).

opaque but at the edges the two gradually diffuse into each other throughout the thickness of the material. If the piece is relatively thin, it is possible to see clusters of melanin-pigmented cells under low magnification and transmitted light. These clusters are spaced increasingly further apart as the edge of the mottling merges with the transparent ground (Fig. 18). Freshly polished, tortoiseshell is entirely smooth but in time, probably through a combination of dehydration and long exposure to light, the edges of the fine layers become visible giving an appearance like watermarked silk where they are cut through by surface working (Fig. 19A).

The condition of archaeological finds of tortoiseshell varies greatly. As deterioration proceeds, the surface layers begin to separate, the cells of the layers begin to degrade, and the bonds between them are disrupted. Groups of cells are lost and the surface develops a whitish, opaque, granular appearance (Fig. 19B). This deterioration proceeds in from the edges of the object along the layers. Eventually the layers are completely reduced to a granular state but the junction between each layer is still marked by the boundary layer (Fig. 19C). This thin film-like layer can persist after the granular material disintegrates, leaving tortoiseshell comb teeth, for instance, with the appearance of the vanes of a miniature fan (Fig. 19D). All of these stages in the deterioration of tortoiseshell were observed together in a single cache of comb-making debris from the site of the nineteenth-century Rougier family comb factory in York.

Of all the keratinous tissues described, tortoiseshell is the most likely to be imitated in other materials because of the high price of this exotic import and these imitations may be recovered from archaeological deposits. Low magnification microscopy can be used to distinguish these from tortoiseshell. Mottling with sharply defined edges, swirls in the pigmentation, and irregular shaped, colored, or reflective particles in the pigmented areas or the pale ground are indicative of a plastic imitation tortoiseshell. Fine, random crazing of the surface also indicates a decayed plastic. If traces of striae are seen within the material this suggests that the material is pressed blond horn used in imitation of tortoiseshell. In this case, any mottled coloration will be limited to the surfaces of the material. Surface-only coloration may also be observed where plainer material from plastron or carapace has been enhanced by painting to imitate more highly prized and priced 'true' tortoiseshell. In addition, thin veneers of tortoiseshell can be bonded to either side of a sheet of pressed, blond horn, as O'Connor has observed on the backs and handles of Victorian hair brushes. This can look very like solid tortoiseshell unless the striae of the horn become visible as the materials deteriorate.

Other approaches to identification

Where researchers have been unfamiliar with the features of these keratinous materials, the evidence is ambiguous or the material badly degraded, several chemical identification techniques have been employed. Wellman (1997) investigated the use of the iodine azide spot test to detect high sulfur protein to help distinguish horn from leather. The test could not distinguish between different sources of keratins or protein and non-protein sources of sulfur. Anheuser & Roumeliotou (2003) were successful in distinguishing microscopic samples of highly degraded animal and plant derived MPO textiles using chemical staining techniques. These stains could separate animal tissue from wood, but could not distinguish collagen from keratin.

Vibrational spectroscopy using infrared light has proven more useful in the identification of keratinous tissues and requires little or no preparation of the specimen. Edwards *et al*. (1998) used Fourier transform Raman spectroscopy (FT-Raman) to distinguish between modern specimens of five different keratinous tissues: bovine hoof and horn, antelope horn, marine turtle shell, and human finger nail, and compared these with commercial bovine keratin powder. The predominance of beta-keratin in the tortoiseshell made it readily distinguishable from the mammalian tissues but the differences between the mammalian tissue spectra were altogether more subtle and a greater number of samples might have shown more variation, reducing the apparent differences between these tissues. Espinoza *et al*. (2007) used diffuse reflectance infrared Fourier transform spectroscopy (DRIFTS) to analyze bovid and sea turtle keratinous tissues and differentiate them from casein, a protein-based plastic historically used in imitation of tortoiseshell. They acquired spectra from 35 bovid horn or hoof specimens representing 24 different species and 24 sea turtle shells or mandibular beaks from four different species. Although DRIFTS has a lower resolution than FTIR, using discriminant analysis it was possible to separate the horn and turtle shell keratin with a performance index of 95.7% and all 59 of the samples were correctly assigned.

Archaeological materials present unique problems for vibrational spectroscopy. Deterioration of the organic components produces spreading of spectral features. At the same time there may be loss of the inorganic component and increased noise from mineral and organic contamination from the burial environment. Together these factors combine to degrade the spectra. An extreme example of this was a poorly preserved cattle claw from waterlogged deposits at York from which FT-Raman failed to gain recognizable keratin spectra. With well-preserved finds it may be possible to separate alpha-keratin from

beta-keratin but only through visual examination of the structural evidence can the identification of the tissue be refined. An example of this combined approach is the use of attenuated total reflectance infrared spectroscopy (ATR) and visual identification criteria to identify a find from the 1718 ship *Queen Anne's Revenge* (Welsh *et al*., 2012). Originally identified as leather, ATR produced a spectrum that, when compared to a range of known samples, strongly resembled known horn. These results only confirmed the object to be a keratinous material but linear corrugations observed upon cleaning supported the identification as horn.

None of these techniques can take the identification of keratinous tissues further than visual identification techniques. aDNA can provide an answer although, depending on the context, this may involve a curatorially unacceptable level of destructive sampling. The DNA primarily derives from the mitochondria that power the high levels of keratin production in the epithelial cells, which ultimately leads to the death of the cells. When the cells die, the DNA is plasticized but remains entrapped within the keratin from where it is very simple to decontaminate (Gilbert *et al*., 2006). Under conditions in which the keratin is well preserved, it is a valuable source of DNA (e.g. Gilbert *et al*., 2007; Clack *et al*., 2012), and has been used in the reconstruction of the first ancient human genome (Rasmussen *et al*., 2010). Biodeterioration of the keratin, however, destroys the protection it affords aDNA, but in such circumstances analysis of surviving keratin protein remnants might still provide an identification. Here we present the results of a pilot study of keratin peptide analysis applied to the problem of differentiating keratinous tissues when diagnostic morphological features cannot be seen.

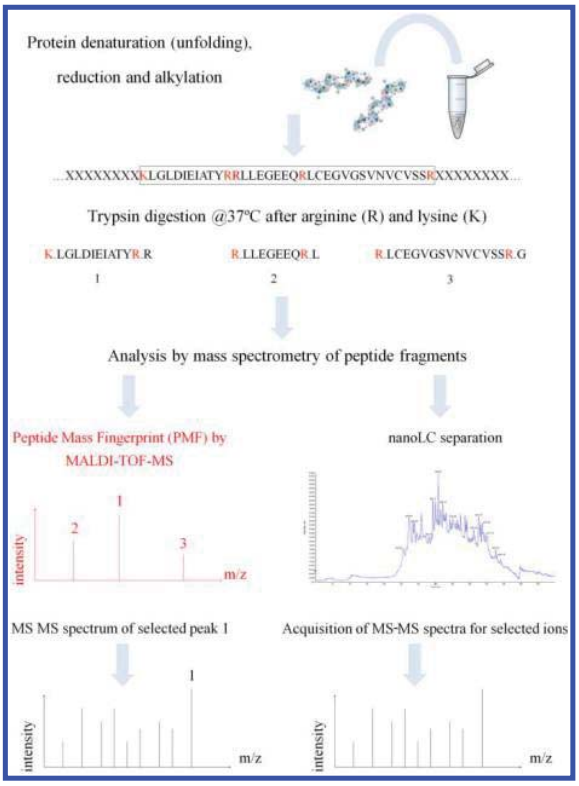

Figure 20 Schematic representation of the preparation and analytical steps for the identification of proteins by mass spectrometry.

Species identification of keratins using peptide mass fingerprinting

Species identification by mass spectrometry is based on the fact that proteins have variable amino acid sequences across taxa, that these amino acids have different chemical compositions and, therefore, different masses. The more two species diverge in evolutionary terms, the more sequence variations are to be expected for a given protein. Enzymatically digested proteins produce a mixture of peptides (short strings of amino acids) that are identified by their mass-to-charge ratio (m/z) using matrix-assisted laser desorption ionization-time of flight-mass spectrometry (MALDI-ToF-MS). Due to the conserved nature of keratins, most of the cleaved peptides will have the same string of amino acids and therefore the same m/z and same peak position. However, if there is one difference in the original protein sequence between two species, the peptide cleaved from this region will have a different m/z in each of the species, and hence peak positions will differ, resulting in a diagnostic peptide marker.

The profile or peptide mass fingerprint (PMF) obtained (Fig. 20) is representative of the analyzed species (Buckley *et al*., 2009, 2010; Collins *et al*., 2010; van Doorn *et al*., 2011). An unknown sample can then be identified by matching its PMF against the PMF of reference samples, usually using several diagnostic peptide markers to validate the identification. PMF has been widely used on collagen from bone and soft tissues and specimens can generally be identified at the genus level but recent studies have shown that some markers were diagnostic to the species level in certain marine mammals (Kirby *et al*., 2013). PMFs of keratin in animal fibers have also been successfully used to identify ancient textiles and cloths (Solazzo *et al*., 2011; Hollemeyer *et al*., 2012).

Prior to digestion, cysteine residues of the extracted keratins are chemically reduced to break the disulfide bridges and alkylated to prevent their reformation. The enzyme trypsin is used to digest the alpha-keratin proteins as it cuts specifically after the basic amino acids arginine (R) and lysine (K), in which alpha-keratins are particularly rich, producing peptides with mass ranges suitable for PMF (typically 800–4000 Da) (Fig. 20). Trypsin is less efficient on the matrix proteins

Table 1 Archaeological keratinous materials sampled for PMF

Origin/site code and finds number (sf)	Object	Material	Condition	Sample size taken for analysis
York Archaeological Trust				
1977.7 sf 16022	Offcut	Horn	(a) Opaque and pale fawn/grey with surviving corrugated lamellar structure, (b) Gelatinized – brittle, brown/black resinous appearance with no surviving structure (Fig. 4)	(a) 13 mg; (b) 5 mg;
1876.13 sf2930	Offcut	Horn	Opaque and pale fawn/gray with surviving corrugated lamellar structure	7 mg
1981.7 sf 11937	Knife handle	Horn	Iron stained MPO remains with surviving corrugated lamellar structure (Fig. 5)	5 mg
1983.32 sf 1349	Comb making debris	Tortoiseshell	Brown, opaque and delaminating into fine layers	10 mg
Worcester archaeology				
WCM100879 sf 60	Comb fragment	Tortoiseshell	Surface layers becoming granular and detached but natural pigmentation and areas of translucency surviving in the core	5 mg

and therefore the alpha-keratin proteins are expressed to a greater degree in the PMF and peptide markers belonging to the most abundant alpha-keratins can provide reliable identification up to the genus level (Solazzo *et al.*, 2013b). The wool (or hair), horn, and hoof of an animal produce the same keratin sequences but, due to variations in protein expression, differences can be identified between some species markers in 'soft' and 'hard' tissues (Solazzo *et al.*, 2013b). Trypsin is less well adapted to beta-keratin digestion as these keratins contain less of the basic residues. However, the proteolytic action of trypsin on beta-keratins is sufficient to identify major markers and when working with unknown keratinous materials a methodology that works indiscriminately on alpha- and beta-keratin is necessary.

Experimental

To explore the potential of PMF for identifying archaeological horn and other keratinous hard tissue remains, samples were collected from five archaeological finds in various states of preservation, previously identified on

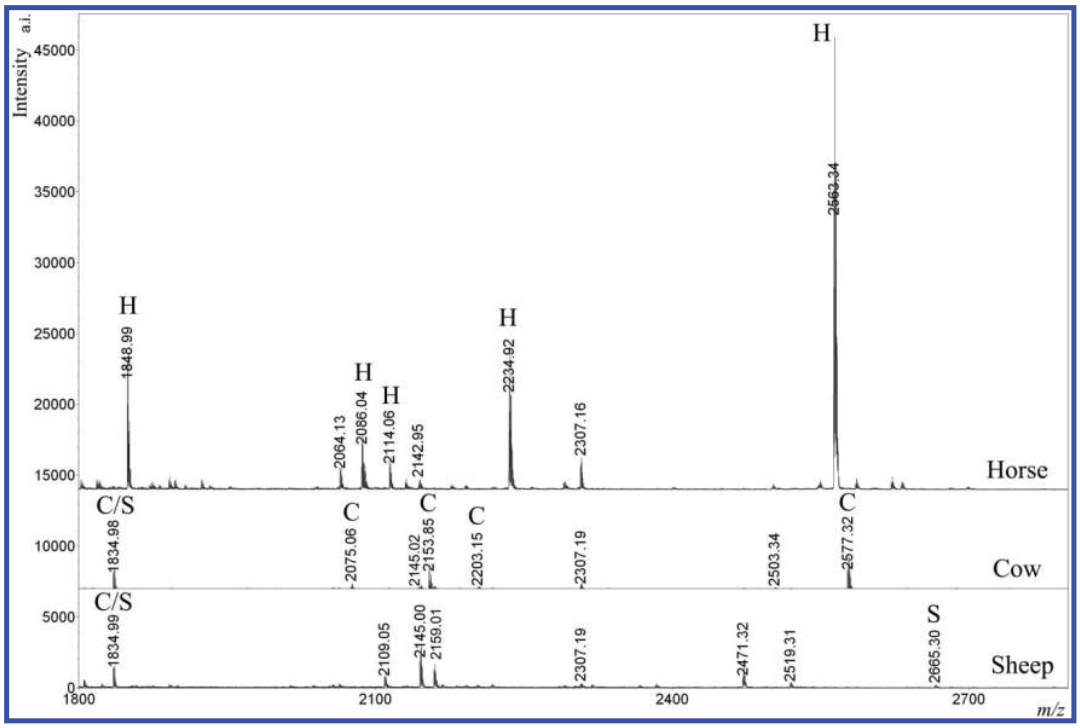

Figure 21 Zoomed area (*m*/*z* 1800–2800 Da) of the PMF of modern samples of sheep horn, cow horn and horse hoof with markers indicated as S (sheep), cow (C) and horse (H).

Table 2 Main markers for differentiating sheep, cow, and horse. $[M+H]^+$ calculated with carboxymethylation of cysteine (+58 Da on C)

$[M+H]^+$	Peptide sequence	Sheep (*Ovis aries*)	Cow (*Bos taurus*)	Horse (*Equus caballus*)
952.50	LQFFQNR	S		
968.49	LQFYQNR	S	C	H
1041.49	WQFYQNR			H
1109.53	DVEEWYIR	S	C	
1896.86	DVEEWFTTQTEELNR			H
1834.98	**TVNALEVELQAQHNLR**	**S**	**C**	
1848.99	**TVNALEIELQAQHNLR**			**H**
2063.03/2191.12	SDLEANSEALIQEIDFLR/KSDLEANSEALIQEIDFLR	S	C	
2075.06/2203.16	**SDLEANVEALIQEIDFLR/KSDLEANVEALIQEIDFLR**		**C**	
2086.04	**LEAAVSQAEQQGEVALTDAR**			**H**
2114.07	**LEVAVSQAEQQGEVALTDAR**			**H**
2144.97	SQQQEPLVCPNYQSYFR	S	C	
2234.91	**CQQQEPEVCPNYQSYFR**			**H**
2563.34	**YSSQLSQVQGLITNVESQLAEIR**			**H**
2577.30	**YSCQLAQVQGLIGNVESQLAEIR**		**C**	
2665.35	**YSCQLSQVQSLIVNVESQLAEIR**	**S**		
2154.07	**GDLEANAHSLVEEVCVLGLK**		**C**	

In bold, markers indicated on Fig. 21.

their visible structures by O'Connor (Table 1 and Figs. 4, 5, and 19B). These were compared with the PMFs gained from modern cow horn, sheep horn, and horse hoof, and well-preserved historic tortoiseshell of hawksbill and green turtle, from the teaching collection of the University of Bradford. Sampling of the finds was kept to a minimum, between 5 and 13 mg, and done as discreetly as possible to reduce visual impact. The samples of comparandum specimens were of a similar size, between 9 and 15 mg. Details of the sample preparation and analytical procedure are given in the Appendix.

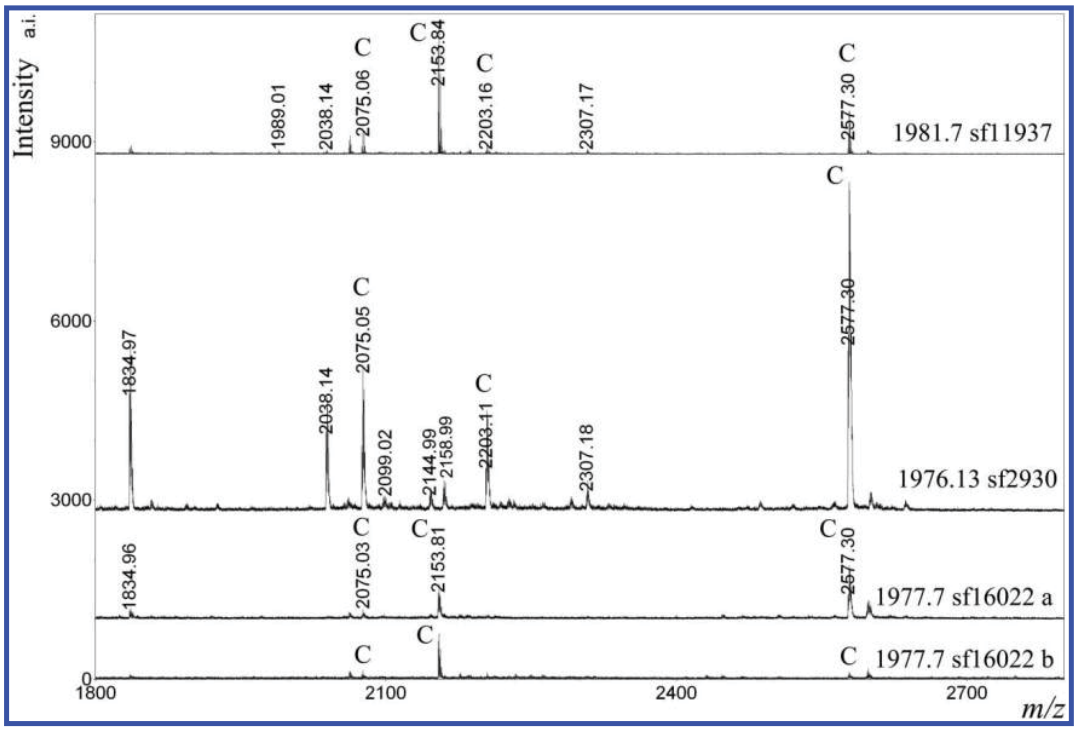

Figure 22 Zoomed area (*m*/*z* 1800–2800 Da) of the PMF of the archaeological samples 1977.7 sf16022 a (flake) and b (gelatinized), 1976.13 sf2930 and 1981.7 sf11937 with cow markers indicated as C.

Results

Horn and hoof: alpha-keratins

While it is preferable to identify a combination of markers for reliable identification, some unique markers have been found to be diagnostic to the genus level (Solazzo *et al*., 2013b) and therefore can be used to discriminate the most common taxa. Fig. 21 shows the main markers used for species identification in horse, cow, and sheep gained from the comparandum specimens and Table 2 gives the peptide sequences for these peaks. A complete list of markers can be found in Solazzo *et al*. (2013b) where sheep horn, cow horn, and horse hoof were compared to their wool or hair equivalents.

The same diagnostic area is shown in Fig. 22 for the archaeological samples. All these samples match cattle horn, confirming the visual identifications. All but one sample displays three cow diagnostic peaks at m/z 2075, 2154, and 2577. In 1976.13 sf2930, peak m/z 2154 is missing but there is a peak at m/z 2203, which is also present in 1981.7 sf1937.

Turtle: beta-keratins

As limited sequence information was available for green and hawksbill turtles, nanoLC-ESI-MS-MS (liquid chromatographic separation of peptides and fragmentation of the entities in their amino acid sequences) data were obtained and peaks from their respective PMFs matched to a sequence (when possible) by comparison with available sequences from other turtle species (Tables 3 and 4). The green turtle (*Chelonia mydas*) and the hawksbill turtle (*Eretmochelys imbricate*) belong to the Cheloniidae family of marine turtles but to two different genera.

Table 3 Proteins identified in green turtle by nanoLC-ESI-MS-MS, for which more than two peptides were matched to a score > 30 (some peptides are present in more than one proteins)*

Accession number†	Mr	Error (ppm)	Score	Sequence	Reported modifications with error tolerant	Error tolerant sequence	Peaks present on PMF $[M+H]^+$
gi/215541341	905.3735	−1.82	33	T.CNEPCVR.Q	E3 → V	T.CNVPCVR.Q	
	1133.494	6.56	62	G.LCGSGVSCHR.Y			
	1185.536	2.84	55	R.QCPDSEVVIR.P	Gln- > pyro-Glu (N-term Q)		1186.52
	1190.4808	−0.82	60	G.GLCGSGVSCHR.Y			
	1202.5601	0.36	69	R.QCPDSEVVIR.P			1203.57
	1247.5023	1.15	62	Y.GGLCGSGVSCHR.Y			
	1399.5748	1.56	51	F.SSLCYPECGVAR.P			
	1402.6630	3.6	46	Y.GGLYGLGGYGGYGGR.Y			
	1467.5871	4.13	57	Y.GYGGLCGSGVSCHR.Y			
	1560.6549	10.4	90	R.PSPVTGTCNEPCVR.Q	T7 → S	R.PSPVTGSCNEPCVR.Q	1561.7
	1617.6803	3.56	61	M.TFSSLCYPECGVAR.P	T1 → A	M.AFSSLCYPECGVAR.P	
	1647.6909	3.79	65	M.TFSSLCYPECGVAR.P			
	1659.6909	−4.78	74	M.TFSSLCYPECGVAR.P	Acetyl (Nterm); T1 → A	M.AFSSLCYPECGVAR.P	1660.71
	1687.6719	−10.18	48	G.GYGYGGLCGSGVSCHR.Y			
	1744.6934	−8.79	46	L.GGYGYGGLCGSGVSCHR.Y			
	1781.7462	6.94	102	Y.LGGYGYGGLCGSGVSCHR.Y	Y6 → S	Y.LGGYGSGGLCGSGVSCH	
gi|215541525	**1524.6086**	6.13	72	Y.GGYGGLCGSGVSCHR.Y			
	1530.6620	9.37	65	R.PSPVTGSSNEPCVR.Q	Carboxy E10		1531.7
gi|215541337	713.3497	14.4	40	G.YGGYGR.R	G3 → V	G.YGVYGR.R	
	728.3242	2.66	30	W.GYGGYGR.R			
	928.4403	−1.92	36	L.YGGLYGLGR.L	L4 → S	L.YGGSYGLGR.L	
	954.4923	−6.98	65	L.YGGLYGLGR.L			955.51
	1651.799	−6.06	50	G.GYGYGGLYGGLYGLGR.L	G3 → S	G.GYSYGGLYGGLYGLGR.L	1652.81
gi|215541529	1199.5492	−10.1	60	R.QCPDSEVIIR.P	Gln → pyro-Glu (N-term Q)		
	1216.5758	11.3	55	R.QCPDSEVIIR.P			1217.6
	1546.6392	9.62	69	R.PSPVSGSCNEPCVR.Q			1547.66

*Are shown: accession number from NCBI (National Center for Biotechnology Information, USA), molecular weight Mr, error in ppm of the identified peptides, their score (Mascot), sequence, and modifications and adjusted sequence obtained after running error tolerant.
†All proteins identified are 'beta-keratin-like protein [Pseudemys nelsoni]' from the Florida redbelly turtle. Finally peaks identified on PMFs are indicated and in bold are markers found in both green and hawksbill turtles.

Table 4 Proteins identified in hawksbill turtle by nano-LC-ESI-MS-MS.

Accession number†	Mr	Error (ppm)	Score	Sequence	Reported modifications with error tolerant	Error tolerant sequence	Peaks present on PMF $[M+H]^+$
gi|215541525	**1190.4808**	−1.88	42	G.GLCGSGVSCHR.Y			
	1247.5023	−2.77	73	Y.GGLCGSGVSCHR.Y			
	1467.5871	−2.41	71	G.GYGGLCGSGVSCHR.Y			
	1524.6086	8.40	43	Y.GGYGGLCGSGVSCHR.Y			
	1530.6620	4.37	63	R.PSPVTGSSNEPCVR.Q	Carboxy E10		**1531.73**
	1647.6909	1.77	58	M.TFSSLCYPECGVAR.P			
	1670.7108	−3.63	73	G.GYGGYGGLCGSGVSCHR.Y	C9 → S	G.GYGGYGGLSGSGVSCHR.Y	
	1744.6934	3.62	71	G.GYGGYGGLCGSGVSCHR.Y			
	1801.7148	3.50	53	L.GGYGGYGGLCGSGVSCHR.Y			
	1914.7989	−2.24	87	G.LGGYGGYGGLCGSGVSCHR.Y			
	2800.1719	−1.61	57	G.SGGHYGGLSGLGGYGGYGGLCGSGVSCHR.Y	Carbamyl (N-term); S9 → G	G.SGGHYGGLGGL GGYGGYGGLCGS GVSCHR.Y	2801.33
gi|215541341	**1202.5601**	8.99	75	R.QCPDSEVVIR.P			
	1579.7420	2.80	71	L.YGGLYGLGGYGGYGGR.Y	G11 → A	L.YGGLYGLGGYAGYGGR.Y	1580.71
gi|215541339	1233.5659	−0.91	79	R.QCQDSEVVIR.P			
gi|215541337	**728.3242**	−1.95	45	W.GYGGYGR.R			
	791.4290	0.21	47	Y.GGLYGLGR.Y			
	954.4923	0.19	65	L.YGGLYGLGR.L			**955.51**
	997.4981	10.8	64	L.YGGLYGLGR.L	Carbamyl (N-term) Acetyl (Nterm); Oxidation Y1		1013.53
	1012.4978	2.23	50	L.YGGLYGLGR.L			
gi|215541529	1068.5353	3.17	49	F.GLGGLYGYGGH.Y	H11 → R	F.GLGGLYGYGGR.Y	
	1189.5516	−1.45	72	R.YGYGGLSGYGGR.Y	Y3 → F	R.YGFGGLSGYGGR.Y	1190.61
	1215.6037	−3.8	52	S.FGLGGLYGYGGH.Y	H12 → R	S.FGLGGLYGYGGR.Y	
	1216.5758	−0.06	59	R.QCPDSEVIIR.P			
	1235.5571	12.1	86	R.YGYGGLSGYGGR.Y	G8 → S	R.YGYGGLSSYGG	1236.6
	1278.5629	−4.66	56	R.YGYGGLSGYGGR.Y	Carbamyl (N-term); G8 → S	R.YGYGGLSSYGGR.Y	
	1302.6357	−10.21	42	G.SFGLGGLYGYGGH.Y	H13 → R	G.SFGLGGLYGYGGR.Y	
	1359.6572	−4.70	68	G.GSFGLGGLYGYGGH.Y	H14 → R	G.GSFGLGGLYGYGGR.Y	
	1416.6787	−2.94	82	Y.GGSFGLGGLYGYGGH.Y	H15 → R	Y.GGSFGLGGLYGYGGR.Y	
	1532.6929	6.08	74	R.PSPVSGSCNEPCVR.Q	C8 → F	R.PSPVSGSFNEPCVR.Q	

gi|215541331	945.3902	3.89	36	G.YGGLCGSGV.S	S7→ Y	G.YGGLCGYGV.S	
	1560.6549	4.38	70	R.PSPVTGTCNEPCVR.Q	T7 → S	R.PSPVTGSCNEPCVR.Q	**1561.61**
	1617.6803	−1.05	74	M.TFSSLCYPECGVAR.P	S4→ G	M.TFSGLCYPECGVAR.P	
	1659.6909	−8.09	48	M.TFSSLCYPECGVAR.P	Acetyl (Nterm); S4 → G	M.TFSGLCYPECGVAR.P	**1660.76**
	2191.9052	0.71	51	L.GGYLGGYGYGGLCGSGVSCHR.Y		L.GGYLGGYGYGGGLCGSGVSCHR.Y	
	2419.322	−4.78	51	Y.GGLGGYLGGYGYGGLCGSGVSCHR.Y		YGGGLCGSGVSCHR.Y	
	2639.1170	−8.35	74	Y.GGLGGYLGGYGYGGLCGSGVSCHR.Y	+57(G)→ G16	Y.GYGGLGGYLGGYGYGGGLCGSGVSCHR.Y	

It is therefore expected to see a substantial difference in the peptide profiles between genera as is seen between alpha-keratin-made tissues. Fig. 23 indicates the unique markers (unique, that is, in this two-taxon comparison) identified for green turtle and Fig. 24 those for hawksbill turtle (see Discussion).

The profiles of the archaeological tortoiseshell samples are included in Fig. 24 as they matched the hawksbill turtle better than the green turtle. In particular, sample WCM100879 sf60 has all m/z 1190, 1236, 1580, and 2200 markers but showed none of the green turtle markers. Sample 1983.32 sf1349 showed more signs of degradation with less peaks and only m/z 2200 as a major peak and m/z 1630 as a minor peak, still matching Hawksbill turtle best of the species available as comparanda.

Discussion

Strategies of identification by mass spectrometry

Cow, sheep, and horse are well-sequenced species, for which alpha-keratin sequences are now available through public databases. Markers to separate all three species have been described elsewhere (Solazzo *et al*., 2013b) and are summarized in Table 2, but we focused here on the most diagnostic region of the peptide profiles, between m/z 1800 and 2800 Da. One marker in particular is diagnostic of sheep at m/z 2665, its equivalent in goat is at m/z 2692. The equivalent marker in horse is found at m/z 2563 and in cow at m/z 2577. Cow has two more reliable markers at m/z 2154 and at m/z 2075/2203 (m/z 2203 is one residue longer than m/z 2075), and horse three at m/z 2086, 2114 and 2235 (Table 2).

For turtle beta-keratins, available sequences are limited in the public database to incomplete sets of sequences from the Florida redbelly turtle (18 sequences) and green turtle (two sequences). MS-MS data searched against all animals logically matched beta-keratins from Florida redbelly turtle (Tables 3 and 4). In addition, a few alpha-keratin-like proteins were observed in hawksbill turtle (data not shown) but only beta-keratin peptides were identified on PMF (which allows only a snapshot of the total protein content), most likely due to the alpha-keratins being in the minority.

To increase the chances of matching peptides, the MS-MS dataset was searched against 'error tolerant', a search parameter which uses all possible post-translational modifications as well as possible substitutions of amino acids to match sequences in the proteins identified (here the different beta-keratin-like protein from the Florida redbelly turtle). A high number of peptides were successfully identified through substitutions of amino acids; however, these identifications have to be taken with caution until more sequences

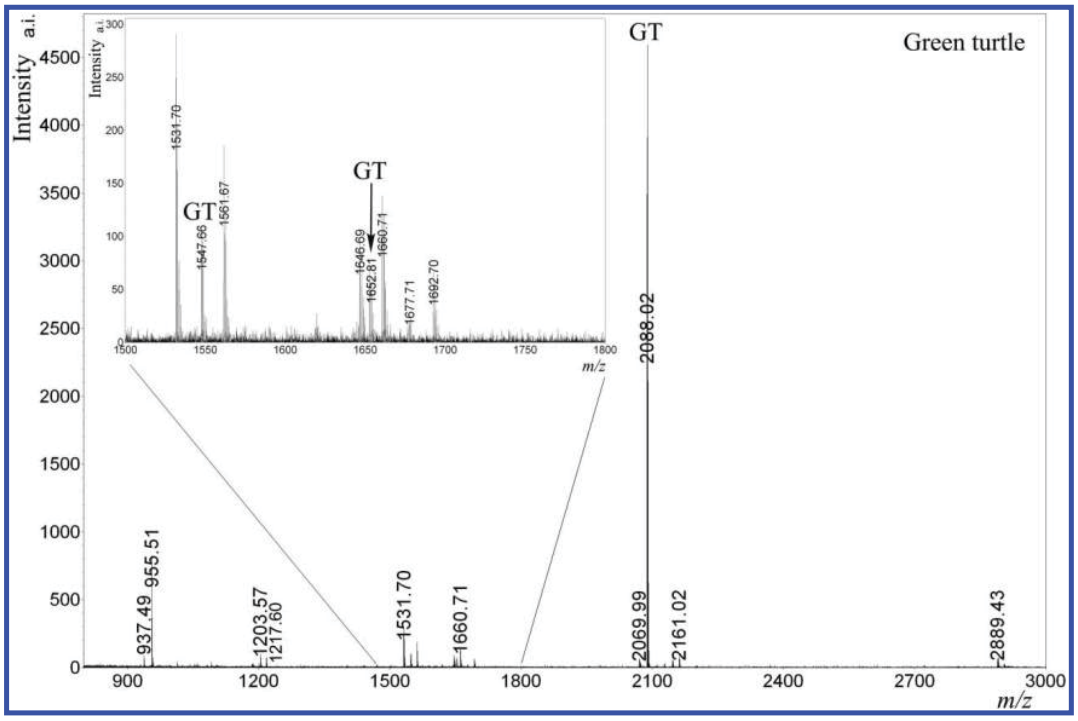

Figure 23 PMF *m*/*z* 800–3000 Da of the green turtle with markers indicated as GT.

are made available. Fortunately, the recent sequencing of the soft-shell turtle *Pelodiscus sinensis*, the green turtle, and the western painted turtle *Chrysemys picta bellii* (Li *et al*., 2013; Shaffer *et al*., 2013; Wang *et al*., 2013) should increase the number of keratin sequences available. Using error tolerant, however, many peptides could be related to beta-keratin sequences, and major peaks observed on the PMFs of both species of turtles could also be associated to a sequence. On the PMFs, four peaks were found in common between green and hawksbill turtles but this number increased to 14 after LC-MS-MS analysis

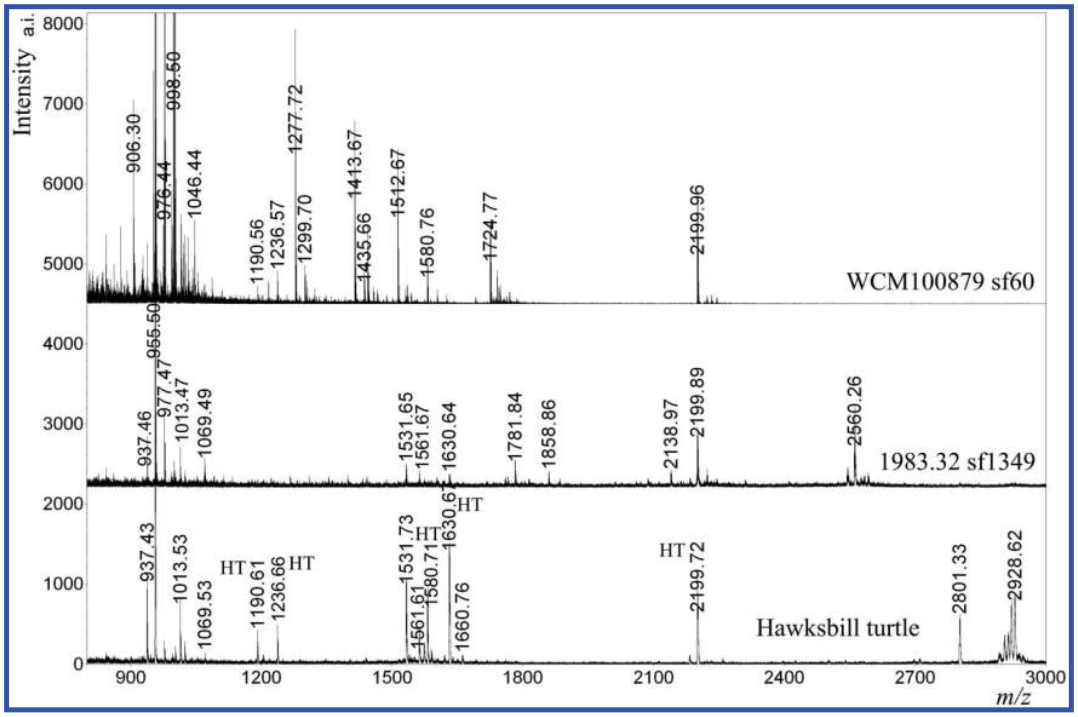

Figure 24 PMF *m*/*z* 800–3000 Da of the hawksbill turtle and archaeological samples WCM100879 sf60 and 1983.32 sf1349 with markers indicated as HT.

Table 5 Peak intensity ratios as compared to *m/z* 2577 (= 1)

	1835/ 2577	2075/ 2577	2154/ 2577	2203/ 2577	2577
Modern cow	0.65	0.13	0.78	0.07	1
1981.7 sf11937	0.16	0.54	**4.76**	0.21	1
1976.13 sf2930	0.49	0.41	0	0.29	1
1977.7 sf16022a	0.17	0.14	0.64	0	1
1977.7 sf16022b	0.54	0.83	**7.34**	0.67	1

(in bold, Tables 3 and 4). Two such peptides, common to both species in LC-MS-MS runs, were observed on the green turtle PMF but not the hawksbill's. Using these complementary methods, diagnostic markers could be established for both turtles: *m/z* 1547 and *m/z* 1652 for green turtle, and *m/z* 1190, *mz* 1236, and *m/z* 1580, for hawksbill turtle. Three major peaks were not identified to a sequence but were found in both LC-MS-MS and PMFs: *m/z* 2088 for green turtle and *m/z* 1630 and *m/z* 2200 for hawksbill turtle (Figs. 23 and 24).

Degradation of hard keratinous tissues

Identification to cow is possible thanks to several markers; however, loss of some peptides and variable proportions of these markers show variable degradation of the archaeological samples (Table 5). In modern cattle horn, *m/z* 1835, 2154, and 2577 are the most intense peaks with much lower *m/z* 2075 and 2203. In 16022a the proportion is maintained except for *m/z* 1835 that loses a lot of intensity and in the gel all peaks become very low compared to *m/z* 2154. In 11937, *m/z* 2154 is also the most intense peak followed by *m/z* 2577, while in 2930 *m/z* 2154 is absent but the intensity of *m/z* 2075 and 2203 are higher. Generally, during degradation there is a loss of some of the most intense peaks (*m/z* 1835 and 2577) and consequently a relative increase of the low intensity peaks at *m/z* 2075 and 2203 with *m/z* 2075 consistently more intense than *m/z* 2203.

Conclusions

On the vast majority of archaeological sites, the harvesting and working of keratinous hard tissues is evidenced largely by secondary indicators, such as caches of boney horn cores. Where these materials do survive it is generally in circumstances where the macro or micro environment has resulted in the inhibition of biodeterioration. As intimate contact with corroding metals is the most frequent preservation mechanism (MPO remains) for these materials in temperate zone, free-draining sites, the evidence for their exploitation prior to the Bronze Age is particularly poor. Their 'invisibility' in the archaeological record is compounded by a lack of familiarity with their structural features and working properties. Today horn and hoof have largely been superseded as raw materials by modern metal alloys and plastics whilst conservation concerns have made the use of baleen and tortoiseshell unavailable and unacceptable.

This paper illustrates how low power microscopy in combination with high quality, directional lighting provides a powerful tool enabling the differentiation and identification of all these keratinous tissues on the basis of structural criteria and characteristic patterns of deterioration without the need for destructive sampling or surface preparation. Horn, hoof, baleen, and tortoiseshell can all be differentiated from each other but identification to species is not always feasible. While cattle horn can be separated from that of sheep/goat horn with some confidence, even when quite decayed, tortoiseshell cannot normally be attributed to the hawksbill or green turtle by these techniques unless the material has retained its translucency and a sufficiently large area has survived to allow the characteristics of the mottled patterning to be observed.

The results presented here demonstrate that peptide mass fingerprinting has the capability to identify degraded keratinous remains to species even when preservation is largely due to mineral replacement or when the fibrous protein has been reduced to a gel by diagenetic changes. This analytical technique does require destructive sampling but the small sample size, typically no bigger than half a grain of rice, should make it curatorially acceptable in the majority of cases where species identification is critical. When proteins break down, the chances of detecting species markers decrease. Identification therefore often depends more on the state of the material than on the size of the sample; there is no analytical gain in increasing the sample size. If PMF fails, an alternative method would be to use nano-LC-MS-MS that not only allows the identification of a higher number of peptides through chromatographic separation and concentration of the samples; it also allows the amino acid sequence of peptides to be 'read', guaranteeing a correct identification of peptides.

What PMF currently cannot do is distinguish between different keratinous tissues of the same species, such as cattle horn from cattle hoof. Used in conjunction with visual identification criteria, however, PMF has the potential to obtain identifications from even highly worked and degraded materials with a level of confidence not previously available.

Acknowledgements

We thank Cluny Chapman, the Hawley Collection, the Horniman Museum, Hull Museums, Leeds Museum

and Galleries, and the York Archaeological Trust for access to the specimens used in this paper. Other than Fig. 1, for which we thank the Canadian Conservation Institute, all photographs are by O'Connor and all analytical graphics are by Solazzo. The research by O'Connor to evaluate and develop techniques for the identification of keratinous hard tissues was undertaken as part of her post-doctoral fellowship, *Cultural Objects Worked in Skeletal Hard Tissues*, funded by the Arts and Humanities Research Council and the Engineering and Physical Sciences Research Council, through their Science and Heritage Programme. Solazzo's work was supported by a Marie Curie International Outgoing Fellowship (FP7-PEOPLE-IOF-GA-2009-236425, THREADs) jointly between University of York, UK, and AgResearch, NZ (2009–2012), and a Smithsonian's Museum Conservation Institute (MCI) post-doctoral grant. Analyses were carried out at The Centre of Excellence in Mass Spectrometry, University of York, supported by Science City York and Yorkshire Forward, using funds from the Northern Way Initiative. We particularly thank Dr. David Ashford for carrying out analyses on the maXis instrument.

Appendix

Chemicals

Urea, tris(2-carboxyethyl)phosphine (TCEP), iodoacetic acid (IAA), ammonium bicarbonate (AB), formic acid, and trifluoroacetic acid (TFA) were provided by Sigma-Aldrich (St Louis, Missouri, USA), acetonitrile (ACN) and acetone by Fisher Scientific (Loughborough, Leicestershire, UK), ethanol (EtOH) by AnalaR NORMAPUR (Lutterworth, Leicestershire, UK), trypsin by Promega (Madison, Wisconsin, USA), and alpha-cyano-4-hydroxycinnamic acid (CHCA) by Bruker Daltonics (Bremen, Germany). The 3500 MWCO Slide A Lyzer® Mini Dialysis units were obtained from Thermo Scientific (Rockford, Illinois, USA).

Sample preparation

Samples were ground to a fine powder in a mortar with the help of liquid nitrogen and allowed to dry overnight, then solubilized by shaking overnight in a solution of 8 M urea, 50 mM Tris, and 50 mM TCEP at pH 8.3. An aliquot of the supernatant was alkylated with 150 mM IAA and vortexed for four hours in the dark. This was followed by 24 hours dialysis with 100 mM AB on 3500 MWCO dialysis units (two changes). The dialyzed aliquot was then digested overnight with 0.5 μg of trypsin at 37°C. Samples were then dried down and re-solubilized in 10 μl of 0.1% TFA.

Peptide mass fingerprinting by MALDI-TOF-MS

A matrix solution was prepared by diluting 0.1 mg of CHCA in 97/3 (acetone/0.1% TFA) and 1 μl was applied onto an AnchorChip™ target (Bruker) and allowed to dry. A 1 μl aliquot of analytical solution was applied and removed after one minute followed by 1 μl of washing buffer (0.1% TFA). The residual droplet was removed and 1 μl of recrystallization solution (0.1 mg of CHCA in 6/3/1 (EtOH/acetone/0.1% TFA)) applied. The plate was loaded in a Ultraflex™ III mass spectrometer (Bruker), and analyses were carried out in positive reflector mode using a Nd:YAG laser operating at 355 nm. Spectra were acquired using flexControl 3.0 (Bruker) on a mass range of m/z 800–4000 Da with an accumulation of 500 shots on the standards and 1000 shots on the samples. The calibration standard (Bruker) was prepared according to the manufacturer's instructions for instrument calibration and consisted of angiotensin I, ACTH clip(1–17), ACTH clip(18–39), and ACTH clip(7–38) peptides.

Peptide analysis by nano-LC-ESI-MS-MS

Analyses of the reference samples were performed on a UHR Q-TOF. HPLC was performed using a nanoAcquity UPLC system (Waters) equipped with a nanoAcquity Symmetry C18, 5 μm trap (180 μm × 20 mm; Waters) and a nanoAcquity BEH130 1.7 μm C18 capillary column (75 m × 250 mm; Waters). The trap wash solvent was 0.1% aqueous formic acid and the trapping flow rate was 10 μl/minute. The trap was washed for five minutes after sample loading before switching flow to the capillary column. The separation used a gradient elution of two solvents: solvent A (0.1% formic acid) and solvent B (acetonitrile containing 0.1% formic acid). The flow rate for the capillary column was 300 nl/minute, column temperature was 60°C and the gradient profile was as follows: initial conditions 5% solvent B (2 minutes), followed by a linear gradient to 35% solvent B over 20 minutes and then a wash with 95% solvent B for 2.5 minutes. The column was returned to initial conditions and re-equilibrated for 25 minutes before subsequent injections. The nano-LC system was interfaced to a maXis UHR Q-TOF (ultrahigh-resolution quadrupole-time-of-flight) mass spectrometer (Bruker) with a nano-electrospray source fitted with a steel emitter needle (180 μm outside diameter × 30 μm inside diameter; Thermo). Positive-ion MS and CID (collision-induced dissociation) – MS-MS spectra were acquired using AutoMSMS mode. Instrument control and data acquisition were performed using Compass 1.3 SP1 software (micrOTOF control and Hystar, Bruker). Instrument settings were: ion spray voltage, 1400 V; dry gas, 4 l/minute; dry gas temperature, 160°C; and ion acquisition range m/z, 50–2200. AutoMSMS

settings were for MS 0.5 seconds (acquisition of survey spectrum) and for MS-MS (CID with N_2 as collision gas) ion acquisition range m/z 350–1400; 0.1 second acquisition for precursor intensities above 100,000 counts; for signals of lower intensities down to 1000 counts acquisition time increased linearly to 1.5 seconds; the collision energy and isolation width settings were automatically calculated using the AutoMSMS fragmentation table; three precursor ions; absolute threshold 1000 counts; preferred charge states 2–4; singly charged ions excluded. Two MS-MS spectra were acquired for each precursor and previously selected target ions were excluded for 60 seconds. Spectra were calibrated using a lock mass signal (m/z 1221.99064) prior to compound detection and peak list creation using DataAnalysis (Bruker Daltonics).

The peak list files obtained were submitted for database searching to a locally running copy of Mascot (Matrix Science Ltd., version 2.3.02). Mascot (Matrix Science) was used to search for matches against the database of publicly available sequences NCBI (National Center for Biotechnology Information, US). Searches were carried out using semi-trypsin as enzyme (horn and hoof) or no enzyme (turtles), two missed cleavages, peptide mass tolerance (MS) of 20 ppm, and fragment mass tolerance (MS-MS) of 0.1 Da, carboxymethylation as a fixed modification (alkylation using IAA adds a +58 Da to the mass of the cysteine residues) and acetyl (N-term), carbamyl (N-term), deamidated (NQ), Gln-> pyro-Glu (N-term Q), Glu-> pyro-Glu (N-term E), and oxidation (M) as variable modifications. Horn and hoof were searched against other mammals while green turtle and hawksbill turtle were searched against all animals.

References

Aguilar, A. 1986. A Review of OldBasque Whaling and Its Effect on the Right Whales (Eubalaena glacialis) of the North Atlantic. *Report of the International Whaling Commission, Special Issue*, 10: 191–9.

Alibardi, L., Dalla Valle, L., Nardi, A. & Toni, M. 2009. Evolution of Hard Proteins in the Sauropsid Integument in Relation to the Cornification of Skin Derivatives in Amniotes. *Journal of Anatomy*, 214: 560–86.

Anheuser, K. & Roumeliotou, M. 2003. Characterisation of Mineralised Archaeological Textile Fibres Through Chemical Staining. *The Conservator*, 27: 23–33.

Armitage, P. 1990. Post-medieval Cattle Horn Cores from the Greyfriars Site, Chichester, West Sussex, England. *Circaea*, 7(2): 81–90.

Bartels, M.H. 2005. The Van Lidth de Jeude family and the Waste from their Privy: Material Culture of a Wealthy Family in 18th-century Tiel, the Netherlands. *Northeast Historical Archaeology*, 34: 5–62.

Beattie, O. & Geiger, J. 1987. *Frozen in Time: The Fate of the Franklin Expedition*. London: Bloomsbury.

Beck, S.W. 1882. *The Drapers' Dictionary. A Manual of Textile Fabrics: Their History and Applications*. London: The Warehousemen and Drapers' Journal Office.

Biek, L. 1963. *Archaeology and the Microscope*. London: Butterworth.

Błyskal, B. 2009. Fungi Utilizing Keratinous Substrates. *International Biodeterioration & Biodegradation*, 63: 631–53.

Bragulla, H. & Hirschberg, R.M. 2003. Horse Hooves and Bird Feathers: Two Model Systems for Studying the Structure and Development of Highly Adapted Integumentary Accessory Organs—The Role of the Dermo-epidermal Interface for the Micro-architecture of Complex Epidermal tructures. *Journal of Experimental Zoology Part B: Molecular and Developmental Evolution*, 298B: 140–51.

Brothwell, D. & Gill-Robinson, H. 2002. Taphonomic and Forensic Aspects of Bog Bodies. In: W.D. Haglund & H.S. Marcella, eds. *Advances in Forensic Taphonomy: Method, Theory, and Archaeological Perspectives*. Boca Raton: CRC Press, pp. 119–33.

Bruce-Mitford, R. & Luscombe, M.R. 1974. The Benty Grange Helmet. In: R. Bruce-Mitford, ed. *Aspects of Anglo-Saxon Archaeology. Sutton Hoo and Other Discoveries*. London: Victor Gollancz Limited, pp. 223–42.

Buckley, M., Collins, M., Thomas-Oates, J. & Wilson, J.C. 2009. Species Identification by Analysis of Bone Collagen Using Matrix-assisted Laser Desorption/Ionisation Time-of-flight Mass Spectrometry. *Rapid Communications in Mass Spectrometry*, 23: 3843–54.

Buckley, M., Whitcher Kansa, S., Howard, S., Campbell, S., Thomas-Oates, J. & Collins, M. 2010. Distinguishing Between Archaeological Sheep and Goat Bones Using a Single Collagen Peptide. *Journal of Archaeological Science*, 37: 13–20.

Campbell Pedersen, M. 2004. *Gem and Ornamental Materials of Organic Origin*. Oxford: Elsevier Butterworth-Heinemann.

Clack, A.A., MacPhee, R.D.E. & Poinar, H.N. 2012. Mylodon Darwinii DNA Sequences from Ancient Fecal Hair Shafts. *Annals of Anatomy=Anatomischer Anzeiger: Official Organ of The Anatomische Gesellschaft*, 194(1): 26–30.

Clark, G. 1947. Whales as an Economic Factor in Prehistoric Europe. *Antiquity*, 21: 84–104.

Collins, M., Buckley, M., Thomas-Oates, J., Wilson, J. & Van Doorn, N., 2010. ZooMS: The Collagen Barcode and Fingerprints. *Spectroscopy Europe*, 11–3.

Collins, M.J., Nielsen-Marsh, C.M., Hiller, J., Smith, C.I., Roberts, J.P., Prigodich, R.V., Wess, T.J., Csapò, J., Millard, A.R. & Turner-Walker, G. 2002. The Survival of Organic Natter in Bone: A Review. *Archaeometry*, 44: 383–94.

Credland, A.G. 1981. Crossbow Remains (Part 2). *Journal of the Society of Archer Antiquaries*, 24: 9–16.

Dalla Valle, L., Michieli, F., Benato, F., Skobo, T. & Alibardi, L. 2013. Molecular Characterization of Alpha-keratins in Comparison to Associated Beta-proteins in Soft-shelled and Hard-shelled Turtles Produced During the Process of Epidermal Differentiation. *Journal of Experimental Zoology Part B: Molecular and Developmental Evolution*, 320(7): 1–14.

Dalla Valle, L., Nardi, A., Toni, M., Emera, D. & Alibardi, L. 2009. Beta-keratins of Turtle Shell are Glycine-proline-tyrosine Rich Proteins Similar to Those of Crocodilians and Birds. *Journal of Anatomy*, 214: 284–300.

Doppelfeld, O. 1964. Das fränkische Knabengrab unter dem Chor des Kölner Domes. *Germania*, 42: 156–88.

Dzierzykray-Rogalski, T. 1986. Natural Mummification in Egypt. In: A.R. David, ed. *Science in Egyptology*. Manchester: Manchester University Press, pp. 101–12.

Edwards, G.M. 1974. *The Preservation of Textiles in Archaeological Contexts*. PhD dissertation, University of London Institute of Archaeology.

Edwards, H.G.M., Hunt, D.E. & Sibley, M.G. 1998. FT-Raman Spectroscopic Study of Keratotic Materials: Horn, Hoof and Tortoiseshell. *Spectrochimica Acta Part A: Molecular and Biomolecular Spectroscopy*, 54: 745–57.

Espinoza, E.O., Baker, B.W. & Berry, C.A. 2007. The Analysis of Sea Turtle and Bovid Keratin Artefacts Using Drift Spectroscopy and Discriminant Analysis. *Archaeometry*, 49: 685–98.

Florian, M.L.E. 1987. Deterioration of Organic Materials Other than Wood. In: C. Pearson, ed. *Conservation of Marine Archaeological Objects*. London: University of Michigan, Butterworths, pp. 21–54.

Franck, A., Cocquyt, G., Simoens, P. & De Belie, N. 2006. Biomechanical Properties of Bovine Claw Horn. *Biosystems Engineering*, 93: 459–67.

Fudge, D.S., Szewciw, L.J. & Schwalb, A.N. 2009. Morphology and Development of Blue Whale Baleen: An Annotated Translation of Tycho Tullberg's Classic 1883 Paper. *Aquatic Mammals*, 35: 226–52.

Gilbert, M.T.P., Djurhuus, D., Melchior, L., Lynnerup, N., Worobey, M., Wilson, A.S., Andreasen, C. & Dissing, J. 2007. DNA from Hair and Nail Clarifies the Genetic Relationship of the 15th Century Qilakitsoq Inuit Mummies. *American Journal of Physical Anthropology*, 133(2): 847–53.

Gilbert, M.T.P., Menez, L., Janaway, R.C., Tobin, D.J., Cooper, A. & Wilson, A.S. 2006. Resistance of Degraded Hair Shafts to Contaminant DNA. *Forensic Science International*, 156(2–3): 208–12.

Gilbert, S.F., Loredo, G.A., Brukman, A. & Burke, A.C. 2001. Morphogenesis of the Turtle Shell: the Development of a Novel Structure in Tetrapod Evolution. *Evolution & Development*, 3: 47–58.

Gillard, R.D., Hardman, S.M., Thomas, R.G. & Watkinson, D.E. 1994. The Mineralization of Fibres in Burial Environments. *Studies in Conservation*, 39: 132–40.

Halstead, L.B. 1974. *Vertebrate Hard Tissues*. London: Wykeham Publications.

Hanausek, T.F. 1907. *The Microscopy of Technical Products*. New York: J. Wiley.

Hashiguchi, K. & Hashimoto, K. 1995. The Mineralization of Crystalline Inorganic Components in Japanese Serow Horn. *Okajimas Folia Anatomica Japonica*, 72: 235–43.

Hashiguchi, K., Hashimoto, K. & Akao, M. 2001. Morphological Character of Crystalline Components Present in Saiga Horn. *Okajimas Folia Anatomica Japonica*, 78: 43–8.

Hett, C. 1980. Unearthed Coins: A Pennyworth of History. *The Journal of the Canadian Conservation Institute*, 4: 21–3.

Hieronymus, T.L., Witmer, L.M. & Ridgely, R.C. 2006. Structure of White Rhinoceros (*Ceratotherium simum*) Horn Investigated by X-ray Computed Tomography and Histology with Implications for Growth and External Form. *Journal of Morphology*, 267: 1172–6.

Hollemeyer, K., Altmeyer, W., Heinzle, E. & Pitra, C. 2012. Matrix-assisted Laser Desorption/Ionization Time-of-flight Mass Spectrometry Combined with Multidimensional Scaling, Binary Hierarchical Cluster Tree and Selected Diagnostic Masses Improves Species Identification of Neolithic Keratin Sequences from Furs of the Tyrolean Iceman Oetzi. *Rapid Communications in Mass Spectrometry*, 26: 1735–45.

Janaway, R. 1983. Textile Fibre Characteristics Preserved by Metal Corrosion: The Potential of S.E.M. Studies. *The Conservator*, 7: 48–52.

Janaway, R.C. 1989. Corrosion Preserved Textiles: Mechanisms, Bias and Interpretation. In: R.C. Janaway & B. Scott, eds. *Evidence Preserved In Corrosion Products: New Fields in Artifact Studies*. London: United Kingdom Institute for Conservation (Occasional Paper 8), pp. 21–9.

Janaway, R.C. & Scott, B. eds. 1983. *Evidence Preserved in Corrosion Products: New Fields in Artifact Studies*. London: United Kingdom Institute for Conservation, Occasional Paper 8.

Jones, M. 2003. *For Future Generations: Conservation of a Tudor Maritime Collection*. Portsmouth: Mary Rose Trust Limited.

Keepax, C. 1975. Scanning Electron Microscopy of Wood Replaced by Iron Corrosion Products. *Journal of Archaeological Science*, 2: 145–50.

Kirby, D.P., Buckley, M., Promise, E., Trauger, S.A. & Holdcraft, T.R. 2013. Identification of Collagen-based Materials in Cultural Heritage. *Analyst*, in press., 138: 4849–58.

Krzyszkowska, O. 1990. *Ivory and Related Materials: An Illustrated Guide*. London: London Institute of Classical Studies (Classical Handbook 3, Bulletin Supplement 59).

Lauffenburger, J.A. 1993. Baleen in Museum Collections: Its Sources, Uses, and Identification. *Journal of the American Institute for Conservation*, 32: 213–30.

Li, Y.I., Kong, L., Ponting, C.P. & Haerty, W. 2013. Rapid Evolution of Beta-Keratin Genes Contribute to Phenotypic Differences That Distinguish Turtles and Birds from Other Reptiles. *Genome Biology and Evolution*, 5: 923–33.

MacGregor, A. 1985. *Bone, Antler, Ivory and Horn: The Technology of Skeletal Materials Since the Roman Period*. London: Croom Helm.

MacGregor, A. 1991. Antler, Bone and Horn. In: J. Blair & N. Ramsay, eds. *English Medieval Industries. Craftsmen, Techniques, Products*. London: The Hambledon Press, pp. 356–78.

Marshall, R.C., Orwin, D.F.G. & Gillespie, J.M. 1991. Structure and Biochemistry of Mammalian Hard Keratin. *Electron Microscopy Reviews*, 4: 47–83.

McKittrick, J., Chen, P.Y., Bodde, S.G., Yang, W., Novitskaya, E.E. & Meyers, M.A. 2012. The Structure, Functions, and Mechanical Properties of Keratin. *JOM Journal of the Minerals, Metals and Materials Society*, 64: 449–68.

McKittrick, J., Chen, P.Y., Tombolato, L., Novitskaya, E.E., Trim, M.W., Hirata, G.A., Olevsky, E.A., Horstemeyer, M.F. & Meyers, M.A. 2010. Energy Absorbent Natural Materials and Bioinspired Design Strategies: A Review. *Materials Science and Engineering C*, 30: 331–42.

Moffat, R., Spriggs, J. & O'Connor, S. 2008. The Use of Baleen for Arms, Armour and Heraldic Crests in Medieval Britain. *The Antiquaries Journal*, 88: 207–15.

Mulville, J. 2002. The Role of Cetacea in Prehistoric and Historic Atlantic Scotland. *International Journal of Osteoarchaeology*, 12: 34–48.

O'Connor, S. 1987. The Identification of Osseous and Keratinaceous Materials at York. In: K. Starling & D. Watkinson, eds. *Archaeological Bone, Antler and Ivory*. London: United Kingdom Institute for Conservation, pp. 9–21.

O'Connor, S. 2013. Exotic Materials used in the Construction of Iron Age Sword Handles from South Cave, UK. In: A. Choyke & S. O'Connor, eds. *From These Bare Bones: Raw materials and the Study of Worked Osseous Objects. Proceedings of the Raw Materials session at the 11th ICAZ Conference, Paris, 2010*. Oxford: Oxbow, pp. 188–200.

O'Connor, S. in press. Exotic Materials Used in the Construction of Iron Age Sword Handles from South Cave, UK. In: A. Choyke & S. O'Connor, eds. *From These Bare Bones: Raw Materials and the Study of Worked Osseous Materials. Proceedings of the Raw Materials Session at the 11th ICAZ Conference, Paris, 2010*. Oxford: Oxbow.

O'Connor, S. & Duncan, H. 2002. The Bone, Antler and Ivory Artefacts. In: I. Roberts, ed. *Pontefract Castle Archaeological Excavations 1982–86*. Leeds: West Yorkshire Archaeology Service, pp. 300–8.

O'Connor, S. & O'Connor, T. In prep. *Reconsideration of the 'Mesolithic Harpoon' from Westward Ho!*. Devon.

Pautard, F.G.E. 1964. Calcification of Keratin. In: A. Rook & R.H. Champion, eds. *Progress in the Biological Sciences in Relation to Dermatology*. London: Cambridge University Press, pp. 227–40.

Pautard, F.G.E. 1970. The Mineral Phase of Calcified Cartilage, Bone and Baleen. *Calcified Tissue Research*, 4: 34–6.

Penniman, T.K. 1952. *Pictures of Ivory and other Animal Teeth, Bone and Antler, Pitt Rivers Museum Occasional Papers on Technology 5*. Oxford: University of Oxford.

Pfeiffer, C.J. 1992. Cellular Structure of Terminal Baleen in Various Mysticete Species. *Aquatic Mammals*, 18: 67–73.

Plowman, J.E. 2007. The Proteomics of Keratin Proteins. *Journal of Chromatography B*, 849: 181–9.

Pollitt, C.C. 2004. Anatomy and Physiology of the Inner Hoof Wall. *Clinical Techniques in Equine Practice*, 3: 3–21.

Rasmussen, M., Li, Y., Lindgreen, S., Pedersen, J.S., Albrechtsen, A., Moltke, I., Metspalu, M., Metspalu, E., Kivisild, T., Gupta, R., Bertalan, M., Nielsen, K., Gilbert, M.T., Wang, Y., Raghavan, M., Campos, P.F., Kamp, H.M., Wilson, A.S., Gledhill, A., Tridico, S., Bunce, M., Lorenzen, E.D., Binladen, J., Guo, X., Zhao, J., Zhang, X., Zhang, H., Li, Z., Chen, M., Orlando, L., Kristiansen, K., Bak, M., Tommerup, N., Bendixen, C., Pierre, T.L., Grønnow, B., Meldgaard, M., Andreasen, C., Fedorova, S.A., Osipova, L.P., Higham, T.F., Ramsey, C.B., Hansen, T.V., Nielsen, F.C., Crawford, M.H., Brunak, S., Sicheritz-Pontén, T., Villems, R., Nielsen, R., Krogh, A., Wang, J. & Willerslev, E. 2010. Ancient Human Genome Sequence of an Extinct Palaeo-Eskimo. *Nature*, 463(7282): 757–62.

Richards, M. 2005. Lighting Equipment. In: J. Gardiner & M.J. Allen, eds. *Before the Mast. Life and Death Aboard the Mary Rose*. Portsmouth: The Mary Rose Trust, pp. 343–8.

Richards, M. & Gardiner, J. 2005. Books and Writing Equipment. In: J. Gardiner & M.J. Allen, eds. *Before the Mast. Life and Death Aboard the Mary Rose*. Portsmouth: The Mary Rose Trust, pp. 127–33.

Rijkelijkhuizen, M. 2008. *Handleiding voor de determinatie van harde dierlijke materialen*. Amsterdam: Amsterdam University Press.

Rijkelijkhuizen, M. 2009. Whales, Walruses, and Elephants: Artisans in Ivory, Baleen, and Other Skeletal Materials in Seventeenth- and Eighteenth-Century Amsterdam. *International Journal of Historical Archaeology*, 13: 409–29.

Ryan, M. 1988. The Irish Horn-reliquary of Tongres/Tongeren, Belgium. In: G. Mac Niocaill & P.F. Wallace, eds. *Keimelia:*

Studies in Medieval Archaeology and History in Memory of Tom Delaney. Galway: Galway University Press, pp. 127–42.

Shaffer, B.H., Minx, P., Warren, D., Shedlock, A., Thomson, R., Valenzuela, N., Abramyan, J., Amemiya, C., Badenhorst, D., Biggar, K., Borchert, G., Botka, C., Bowden, R., Braun, E., Bronikowski, A., Bruneau, B., Buck, L., Capel, B., Castoe, T., Czerwinski, M., Delehaunty, K., Edwards, S., Fronick, C., Fujita, M., Fulton, L., Graves, T., Green, R., Haerty, W., Hariharan, R. & Hernandez, O. 2013. The Western Painted Turtle Genome, a Model for the Evolution of Extreme Physiological Adaptations in a Slowly Evolving Lineage. *Genome Biology*, 14: R28.

Siddons, G.A. 1837. *The Cabinet Maker's Guide*. London: Sherwood, Gilbert and Piper.

Smith, G. 1770. *The Laboratory, or, School of Arts*. London: Crowder and Collins.

Solazzo, C., Dyer, J.M., Clerens, S., Plowman, J.E., Peacock, E.E. & Collins, M.J. 2013a. Proteomic Evaluation of the Biodegradation of Wool Fabrics in Experimental Burials. *International Biodeterioration and Biodegradation*, 80: 48–59.

Solazzo, C., Heald, S., Ballard, M.W., Ashford, D.A., DePriest, P.T., Koestler, R.J. & Collins, M.J. 2011. Proteomics and Coast Salish Blankets: A Tale of Shaggy Dogs? *Antiquity*, 85: 1418–32.

Solazzo, C., Wadsley, M., Clerens, S., Dyer, J.M., Collins, M. & Plowman, J. 2013b. Characterisation of Novel α-keratin Peptide Markers for Species Identification in Keratinous Tissues using Mass Spectrometry. *Rapid Communications in Mass Spectrometry*, 27: 2685–98.

Solomon, S.E., Hendrickson, J.R. & Hendrickson, L.P. 1986. The Structure of the Carapace and Plastron of Juvenile Turtles, Chelonia Mydas (the Green Turtle) and Caretta Caretta (the Loggerhead Turtle). *Journal of Anatomy*, 145: 123–31.

Sorge-English, L. 2011. *Stays and Body Image in London: The Staymaking Trade, 1680–1810*. London: Pickering and Chatto.

Spindler, K. 1993. *The Man in the Ice*. London: Weidenfeld and Nicholson.

Stead, I.M. 2006. *British Iron Age Swords and Scabbards*. London: British Museum.

Stevenson, C.H. 1907. *Whalebone: Its Production and Utilization. Department of Commerce and Labor, Bureau of Fisheries Document #626*. Washington: Government Printing Office.

Stock, S. 1976. *An Introduction to the Identification of Animal and Vegetable Fibres used in Antiquity*. PhD Dissertation, University of London Institute of Archaeology.

Szewciw, L.J., de Kerckhove, D.G., Grime, G.W. & Fudge, D.S. 2010. Calcification Provides Mechanical Reinforcement to Whale Baleen α-keratin. *Proceedings of the Royal Society B: Biological Sciences*, 277: 2597–605.

Tombolato, L., Novitskaya, E.E., Chen, P.Y., Sheppard, F.A. & McKittrick, J. 2010. Microstructure, Elastic Properties and Deformation Mechanisms of Horn Keratin. *Acta Biomaterialia*, 6: 319–30.

Toni, M., Dalla Valle, L. & Alibardi, L. 2007. Hard (Beta-)Keratins in the Epidermis of Reptiles: Composition, Sequence, and Molecular Organization. *Journal of Proteome Research*, 6: 3377–92.

Turgoose, S. 1989. Corrosion and Structure: Modelling the Preservation Mechanisms. In: R. Janaway & B. Scott, eds. *Evidence Preserved In Corrosion Products: New Fields in Artifact Studies*. London: United Kingdom Institute for Conservation (Occasional Paper 8), pp. 30–2.

van Doorn, N.L., Hollund, H. & Collins, M.J. 2011. A Novel and Non-destructive Approach for ZooMS Analysis: Ammonium Bicarbonate Buffer Extraction. *Archaeological and Anthropological Sciences*, 3: 281–9.

Wang, Z., Pascual-Anaya, J., Zadissa, A., Li, W., Niimura, Y., Huang, Z., Li, C., White, S., Xiong, Z., Fang, D., Wang, B., Ming, Y., Chen, Y., Zheng, Y., Kuraku, S., Pignatelli, M., Herrero, J., Beal, K., Nozawa, M., Li, Q., Wang, J., Zhang, H., Yu, L., Shigenobu, S., Wang, J., Liu, J., Flicek, P., Searle, S., Wang, J., Kuratani, S., Yin, Y., Aken, B., Zhang, G. & Irie, N. 2013. The Draft Genomes of Soft-shell Turtle and Green Sea Turtle Yield Insights into the Development and Evolution of the Turtle-specific Body Plan. *Nature Genetics*, 45: 701–6.

Wardlaw, L. & Grant, T. 1994. Treatment of Archaeological Baleen Artifacts at the Canadian Conservation Institute. *Journal of the International Institute for Conservation – Canadian Group*, 19: 31–7.

Watson, J. 1988. Identification of Organic Materials Preserved by Metal Corrosion Products. In: S.L. Olsen, ed. *Scanning Electron Microscopy in Archaeology*. Oxford: Archaeopress. British Archaeological Reports (B.A.R.), pp. 65–76.

Watson, L. 1981. *Sea Guide to Whales of the World*. London: Hutchinson & Co.

Wellman, H. 1997. A Short Note on a Test that Failed. *Conservation News (United Kingdom Institute for Conservation of Historic and Artistic Works)*, 62: 30.

Welsh, W., Biscardi, B., Fink, T., Watkins-Kenney, S. & Kennedy, A. 2012. Identification of Suspected Horn from the Queen Anne's Revenge (1718), North Carolina, USA. *The International Journal of Nautical Archaeology*, 41: 190–3.

Wenham, L.P. 1964. *Hornpot Lane and the Horners of York*. York: Annual Report Yorks Philosophical Society.

West, J. & Credland, A.G. 1995. *Scrimshaw. The Art of the Whaler*. Hull: City Museums and Art Gallery and Hutton Press Ltd.

Whittle, A. 2000. 'Very Like a Whale': Menhirs, Motifs and Myths in the Mesolithic-Neolithic Transition of Northwest Europe. *Cambridge Archaeological Journal*, 10: 243–59.

Wilkinson, R.S. 2003. *Baleen: Its Use as Line Inlay on an 18th Century Chest of Drawers*. Arlington, VA: Wooden Artifacts Group Postprints.

Wilson, A.S., Dodson, H.I., Janaway, R.C., Pollard, A.M. & Tobin, D.J. 2007. Selective Biodegradation in Hair Shafts Derived from Archaeological, Forensic and Experimental Contexts. *British Journal of Dermatology*, 157: 450–7.

Wilson, A.S., Dodson, H.I., Janaway, R.C., Pollard, A.M. & Tobin, D.J. 2010. Evaluating Histological Methods for Assessing Hair Fibre Degradation. *Archaeometry*, 52: 467–81.

Young, S.A. 2012. *The Comparative Anatomy of Baleen: Evolutionary and Ecological Implications*. MSc Thesis, San Diego State University.

Zangerl, R. 1969. The Turtle Shell. In: C. Gans, A. d'Bellairs & T. Parsons, eds. *Biology of the Reptilia*. London: New York Academic Press, pp. 311–39.